Check for updates

*Earthquake Engineering & Structural Dynamics*

WILEY

RESEARCH ARTICLE OPEN ACCESS

# Optimization of Viscoelastic Tuned Mass Damper Systems Subjected to Coloured Excitations

Mario Argenziano[1] | Alessandro Palmeri[2,3] | Angelo Rosario Carotenuto[4] | Elena Mele[4] | Massimiliano Fraldi[4,5]

[1]Department of Engineering, Università degli Studi di Palermo, Palermo, Italy | [2]Department of Structural, Geotechnical & Building Engineering, Politecnico di Torino, Torino, Italy | [3]Anchors Regulations and Code Development, HILTI Entwicklungsgesellschaft mbH, Kaufering, Germany | [4]Department of Structures for Engineering & Architecture, Università degli Studi di Napoli, Napoli, Italy | [5]Laboratoire de Physique de l'École Normale Supérieure ENS, École Normal Supérieure ENS, Paris, France

**Correspondence:** Elena Mele (elenmele@unina.it) | Massimiliano Fraldi (fraldi@unina.it)

**Received:** 11 October 2024 | **Revised:** 28 May 2025 | **Accepted:** 3 July 2025

**Funding:** This study was supported by 'SiciliAn MicronanOTecH Research And Innovation CEnter "SAMOTHRACE" (MUR, PNRR-M4C2, ECS_00000022), spoke 3—University of Palermo 'S2-COMMs—Micro and Nanotechnologies for Smart & Sustainable Communities'; Italian Ministry of University and Research (MUR) through the grant FIT4MEDROB (PNC0000007); National Recovery and Resilience Plan (NRRP) European Union—NextGenerationEU—Project MECHAVERSE P2022M3KKC.

**Keywords:** coloured excitation | $H_2$ optimization | Kanai–Tajimi filter | standard linear solid model | tuned mass damper | viscoelastic damping

## ABSTRACT

In recent decades, there has been growing interest in innovative vibration control strategies to improve the structural reliability of buildings and civil structures against earthquakes, windstorms and other dynamic excitations. One of the most effective methods for reducing dynamic responses is the implementation of tuned mass dampers (TMDs), which leverage the interaction between primary and secondary subsystems. Most optimization procedures in the literature use a Kelvin–Voigt (KV) link to model this interaction. Still, when frequency-dependent devices like viscoelastic dampers and isolation bearings are involved, more refined models should be adopted. This paper extends existing optimization approaches by using the standard linear solid (SLS) model to more accurately represent the connection between the dynamic absorber and the primary structure. We also emphasize the importance of accounting for the damping in the primary system, which is often overlooked but can significantly affect the overall primary–secondary dynamic interaction. Additionally, we explore the sensitivity of optimal TMD parameters to multi-chromatic excitations, which are typically neglected, using the Kanai–Tajimi model to simulate realistic seismic accelerograms. To validate our approach, we performed time-history analyses on lumped-mass models using a selection of natural seismic events, comparing the uncontrolled configurations with KV- and SLS-type TMDs. Our results demonstrate that incorporating the frequency content of seismic inputs is crucial for optimizing the structural control system and show the potential and the effectiveness of our analytical/numerical strategy in facing general viscoelastic TMD design problems considering any kind of seismic excitation.

## 1 | Introduction

Over the past 50 years, engineers and architects have faced increasingly complex challenges in achieving more stringent safety standards for new and existing buildings while minimizing construction costs and reducing the carbon footprint. As a consequence, new materials and structural systems have been proposed and pioneered. For structures exposed to significant dynamic actions such as earthquakes and windstorms, the scientific community has explored various solutions, including base

This is an open access article under the terms of the Creative Commons Attribution License, which permits use, distribution and reproduction in any medium, provided the original work is properly cited.

© 2025 The Author(s). *Earthquake Engineering & Structural Dynamics* published by John Wiley & Sons Ltd.

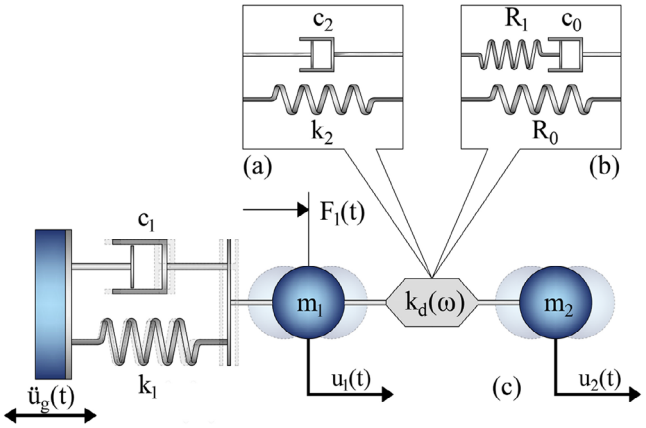


**FIGURE 1** | Kelvin–Voigt (a) and standard linear solid (b) model for the primary-to-secondary mass link in the 2-DoF model of a TMD-controlled structure (c).

and inter-story isolation, re-distribution of masses and lateral resisting systems, energy dissipation devices and the utilization of non-linear dynamic phenomena such as rocking and energy sinks. Within this general framework, the present work employs a combination of analytical and numerical methods to analyse and optimize the dynamic response of structures equipped with tuned mass dampers (TMDs) incorporating linear viscoelastic memory. These linear devices are characterized by 'relaxation' processes in the time domain, leading to frequency-dependent stiffness and damping properties.

As is well-known, a TMD is a secondary mass attached to a structure to control the vibration of the primary system. In classical TMD applications, the dynamic properties of the primary structure are assumed to be known, and the optimization problem consists of finding the mechanical properties of the TMD that minimize the primary system's response to a given dynamic input. Owing to the simplicity of this vibration control strategy, classical TMDs with low secondary-to-primary mass ratios have been widely adopted against wind excitations. More recently, non-conventional TMDs with large mass ratios have been investigated, since it has been demonstrated that they can be very effective in reducing the seismic response of structures under both far- and near-fault earthquake ground motions. Large mass ratios can be easily obtained by employing a part of the structure/building as a dynamic vibration absorber, for example, in the case of inter-story isolation systems (IIS), heavy double-skin façades and mega sub-controlled structures (MSCS) [1–10]. In all these applications, the primary and secondary masses are generally connected through devices incorporating high-damping rubber or other energy dissipation mechanisms and refined mechanical models are required for capturing their viscoelastic behaviour.

Since Den Hartog's seminal work [11], numerous optimization strategies have been proposed for linear TMDs, typically modelled via a Kelvin–Voigt (KV) approach [12–21] (Figure 1a). Conventional TMD designs [13–15] often assume purely viscous damping, neglecting viscoelastic memory effects. Indeed, the role of viscoelasticity in structural dynamics and the effectiveness of dynamic vibration absorbers extend across civil, mechanical and biomedical engineering [22–30].

For non-conventional TMDs, the KV model fails to accurately capture the mechanical behaviour of isolation bearings, which depends on excitation frequency and motion amplitude, as shown experimentally [31]. Therefore, more accurate damping models are thus needed when frequency-dependent materials are used for connecting primary and secondary masses. To address this gap, this paper employs the standard linear solid (SLS) model (Figure 1b), which consists of an elastic spring (representing the quasi-static 'equilibrium modulus') in parallel with a Maxwell element—an elastic spring in series with a viscous dashpot—resulting in frequency-dependent behaviour and fading memory in the time domain. This model is widely used to study stress relaxation and creep in viscoelastic materials, as well as in passive control devices like high-damping elastomeric bearings and fluid viscous dampers [32–38]. For such systems, the complete knowledge of their history before a certain time instant is required [39–41]. Several studies [42–46] have highlighted the limitations of purely viscous damping, as modelled by the KV link. For instance, to overcome these issues, Adhikari and Woodhouse [44] defined new methodologies to identify non-viscous damping models involving an exponentially decaying relaxation function, while Makris and Zhang [45] employed the Biot model to capture the viscoelastic behaviour of soil structures.

The optimization of a dynamic vibration absorber connected via an SLS model to an undamped main system was first studied by Asami and Nishihara [47], who analytically and experimentally characterized an air-damped absorber. Later, they demonstrated that the viscoelastically damped TMD outperforms the conventional KV-type absorber [48]. Starting from the investigations by Xu [49, 50] on the mathematical modelling of the viscoelastic dampers in reducing the earthquake-induced vibrations on civil structures, further studies on SLS-type TMDs have been carried out. Among these, Muresan et al. [51] and Barone et al. [35] employed fractional models to trace back the viscoelastic behaviour of primary-to-secondary mass links. More recently, by using a Den Hartog-inspired *fixed points* approach, Batou and Adhikari [52] derived optimal parameters for the SLS-type TMD, assuming negligible damping in the primary structure.

Although civil engineering structures typically exhibit non-negligible damping, most of the literature on viscoelastically damped TMDs disregards the damping of the primary structure, despite its significant effect on the system's dynamic response. Additionally, aside from the work by Dai et al. [53] where only some specific numerical case studies are provided, the influence of coloured excitations with non-uniform power spectral density (PSD), for example, seismic accelerations, on viscoelastic TMDs is often overlooked. Therefore, despite the fact that the scientific debate is very vivid about this topic, it seems to the best authors' knowledge that a complete and rigorous overview on how optimizing viscoelastic TMDs, considering the damping of primary structures and addressing the specific characteristics of earthquake inputs, is missing. More details on the limitations of the inherent literature and the novelty of the present study are reported in Section 3 of the Supporting Material, where a synoptic comparison between existing procedures and the proposed methodology is illustrated.

To address the limitation above discussed and to establish a comprehensive design methodology for generalised viscoelastic



10969845, 2025, 12, Downloaded from https://onlinelibrary.wiley.com/doi/10.1002/eqe.70025 by Uni Federico II Di Napoli, Wiley Online Library on [17/10/2025]. See the Terms and Conditions (https://onlinelibrary.wiley.com/terms-and-conditions) on Wiley Online Library for rules of use; OA articles are governed by the applicable Creative Commons License

TMD structures subjected to coloured excitations, this study first revisits the classical $H_2$ optimization criterion proposed by Asami et al. [48]. The formulation is reformulated using a novel set of non-dimensional parameters and is extended to incorporate systems with non-negligible primary damping. Specifically, closed-form expressions are derived for the optimal design parameters—two stiffness ratios and a non-dimensional relaxation parameter—under the assumption of zero primary damping, while graphical solutions are provided for cases with nonzero damping. Two canonical excitation scenarios are considered: (i) external force applied to the main mass, representative of wind actions in preliminary design phases, and (ii) base excitation through ground acceleration, modelling seismic input. Within this framework, the performance of optimal SLS-type TMDs is systematically compared to that of traditional KV TMDs. This is done through frequency response analysis and the evaluation of expected values of displacement of the primary masses, even for systems with inherent damping, as further illustrated in the supporting material.

To numerically validate the effectiveness of the proposed methodology, time history analyses have been carried out on lumped mass models by selecting a set of natural seismic accelerograms, showing that SLS-type TMDs almost always perform better than the conventional KV-type ones. Within this framework, the provided analyses are not to be intended as mere parametric analyses of specific case studies but rather as a class of optimal solutions obtainable from considering the application of the same proposed strategy under different conditions.

Finally, to gain further insights into the system's behaviour under coloured excitations, the Kanai–Tajimi (KT) filter is employed to model earthquake inputs, and a heuristic optimization procedure is used to minimize the seismic response of the primary oscillator. Comparisons also in terms of time history responses between optimal configurations derived from white noise inputs and those based on excitations with non-uniform PSD reveal that input frequency content significantly influences the optimization results, and neglecting it can lead to sub-optimal configurations. Although linear elastic assumptions have been considered for obtaining optimal configurations, the validity of the proposed approach has been proved also in the non-linear regime, as detailed in Section 2 of the Supporting Material.

## 2 | Statement of the Problem

### 2.1 | Governing Equations

The dynamics of the SLS-type TMD can be studied through a 2-DoF linear lumped-mass model represented in Figure 1. In a mixed time-frequency domain, the equations of motion of the system subjected to two excitations, that is, the force $F_1(t)$ and the ground acceleration $\ddot{u}_g(t)$, can be written as follows:

$$\begin{cases} (m_1 + m_2)\,\ddot{u}_1(t) + m_2\,\ddot{u}_2(t) + c_1\,\dot{u}_1(t) + k_1\,u_1(t) \\ \quad = F_1(t) - (m_1 + m_2)\,\ddot{u}_g(t) \\ m_2[\ddot{u}_1(t) + \ddot{u}_2(t)] + k_d(\omega)\,u_2(t) = -m_2\,\ddot{u}_g(t) \end{cases} \tag{1}$$

where $m_i$ and $u_i(t)$ are the masses and relative displacements of the two DoFs (i.e., $u_2(t)$ is the displacement of the mass $m_2$ relative to the mass $m_1$), $c_1$ and $k_1$ are the equivalent viscous damping coefficient and elastic stiffness of the primary oscillator and $k_d(\omega)$ is the complex-valued dynamic stiffness of the linear viscoelastic device connecting primary and secondary masses, which in general depends on the frequency of vibration $\omega$.

In the second of Equation (1), the mixed time-frequency product $k_d(\omega)\,u_2(t)$ represents the reaction force $f_d(t)$ experienced by the viscoelastic device. In the frequency domain, this force can be expressed as a complex-valued product:

$$\tilde{f}_d(\omega) = \mathcal{F}[f_d(t)] = k_d(\omega)\,\mathcal{F}[u_2(t)]\,, \tag{2}$$

in which $\mathcal{F}[\cdot]$ is the Fourier Transform.

Alternatively, the reaction force $f_d(t)$ can be expressed in the time domain via a convolution integral:

$$f_d(t) = \int_{-\infty}^{t} \varphi_d(t-s)\,\dot{u}(s)\,ds\,, \tag{3}$$

where the real-valued function $\varphi_d(t)$ is the relaxation function of the viscoelastic device, defined as follows:

$$\varphi_d(t) = \mathcal{F}^{-1}\left[\frac{k_d(\omega)}{\imath\,\omega}\right], \tag{4}$$

in which $\mathcal{F}^{-1}[\cdot]$ is the inverse Fourier transform and $\imath = \sqrt{-1}$ is the imaginary unit.

If the classical KV model is used for the primary–secondary link (Figure 1a), that is, an elastic stiffness $k_2$ in parallel with a viscous dashpot $c_2$, then its dynamic stiffness particularises as $k_{d(KV)}(\omega) = k_2 + \imath\,\omega\,c_2$ and the corresponding relaxation function becomes $\varphi_{d(KV)}(t) = k_2\,\theta(t) + c_2\,\delta(t)$, where $\theta(t)$ is the Heaviside's unit step function and $\delta(t) = d\theta(t)/dt$ is the Dirac's delta function. In both time and frequency domains, the KV model exhibits a neat separation between purely elastic ($\propto k$) and purely viscous ($\propto c$) behaviours, which is not always observed in actual viscoelastic materials and devices.

By adopting the SLS model for the link primary-to-secondary mass (Figure 1b), the dynamic stiffness $k_d(\omega)$ particularises as follows:

$$k_{d(SLS)}(\omega) = R_0 + R_1\,\frac{\imath\,\tau_1\,\omega}{1 + \imath\,\tau_1\,\omega}\,, \tag{5}$$

which depends on three parameters, namely: (i) the equilibrium modulus $R_0$, representing the stiffness of the device when subjected to pseudo-static input; (ii) the rigidity coefficient $R_1$ and relaxation time $\tau_1 = c_0/R_1$, $c_0$ being the damping coefficient of the Maxwell element. More in detail, it is known that when $\tau_1$ tends to $+\infty$, a purely elastic behaviour occurs; conversely, when $\tau_1$ tends to zero, the relaxation function of Equation (4) goes to infinity, thus implying that the link assumes a purely viscous behaviour. In the latter case, hence, the SLS link (Figure 1b) reduces to the KV model (Figure 1a), thus confirming that the SLS link generalizes the classical KV case [45, 54, 55].



10969845, 2025, 12, Downloaded from https://onlinelibrary.wiley.com/doi/10.1002/eqe.70025 by Uni Federico II Di Napoli, Wiley Online Library on [17/10/2025]. See the Terms and Conditions (https://onlinelibrary.wiley.com/terms-and-conditions) on Wiley Online Library for rules of use; OA articles are governed by the applicable Creative Commons License

In the frequency domain, by considering the dynamic stiffness reported in Equation (5), the dynamic response of the primary mass $m_1$ can be calculated as follows:

$$\mathcal{F}[u_1(t)] = H_{11(\mathrm{SLS})}(\omega)\,\mathcal{F}[F_1(t)] \tag{6}$$

where $H_{11}(\omega)$ is the complex-valued frequency response function (FRF) of the first DoF, with units of an inverse stiffness, given by the rational expression:

$$H_{11(\mathrm{SLS})}(\omega) = \frac{N_{11}(\omega)}{D_{11}(\omega)}, \tag{7}$$

in which numerator $N_{11}(\omega)$ and denominator $D_{11}(\omega)$ are the following functions:

$$N_{11}(\omega) = m_2\tau_1\omega^3 - \imath m_2\omega^2 + \omega(-R_0\tau_1 - R_1\tau_1) + \imath R_0 \tag{8a}$$

$$\begin{aligned} D_{11}(\omega) = &- m_1 m_2 \tau_1 \omega^5 + \omega^4(\imath c_1 m_2 \tau_1 + \imath m_1 m_2) + \omega^3(c_1 m_2 \\ &+ k_1 m_2 \tau_1 + m_2 R_0 \tau_1 + m_2 R_1 \tau_1 + m_1 R_0 \tau_1 + m_1 R_1 \tau_1) \\ &+ \omega^2(-\imath c_1 R_0 \tau_1 - \imath c_1 R_1 \tau_1 - \imath k_1 m_2 - \imath m_2 R_0 - \imath m_1 R_0) \\ &+ \omega(-c_1 R_0 - k_1 R_0 \tau_1 - k_1 R_1 \tau_1) + \imath k_1 R_0 \end{aligned} \tag{8b}$$

Analogously, the frequency response of the relative displacement between the two masses can be expressed as follows:

$$H_{21(SLS)}(\omega) = \frac{N_{21}(\omega)}{D_{21}(\omega)} \tag{9}$$

where

$$N_{21}(\omega) = m_2\tau_1\omega^3 - \imath m_2\omega^2;\; D_{21}(\omega) = D_{11}(\omega) \tag{10}$$

Similarly to Equation (6), the frequency-domain solution of the equations of motion in the case of ground excitation can be expressed as follows:

$$\mathcal{F}[u_1(t)] = H_{1\mathrm{g}(\mathrm{SLS})}(\omega)\,\mathcal{F}\left[\ddot{u}_{\mathrm{g}}(t)\right], \tag{11}$$

where $H_{1\mathrm{g}}(\omega)$, with units of a squared time, can be expressed as follows:

$$H_{1\mathrm{g}(\mathrm{SLS})}(\omega) = \frac{N_{1\mathrm{g}}(\omega)}{D_{1\mathrm{g}}(\omega)} \tag{12}$$

in which

$$\begin{aligned} N_{1\mathrm{g}}(\omega) = &\; m_1 m_2 \tau_1 \omega^3 - \imath m_1 m_2 \omega^2 + \omega(-m_1 R_0 \tau_1 - m_2 R_0 \tau_1 \\ &- m_1 R_1 \tau_1 - m_2 R_1 \tau_1) + \imath m_1 R_0 + \imath m_2 R_0;\; D_{1\mathrm{g}}(\omega) \\ = &\; D_{11}(\omega) \end{aligned} \tag{13}$$

Finally, the transfer function of $u_2(t)$ in the case of ground excitation $\ddot{u}_{\mathrm{g}}(t)$ can be calculated as follows:

$$H_{2\mathrm{g}(\mathrm{SLS})}(\omega) = \frac{N_{2\mathrm{g}}(\omega)}{D_{2\mathrm{g}}(\omega)}, \tag{14}$$

where

$$N_{2\mathrm{g}}(\omega) = \imath c_1\, m_2\tau_1\omega^2 + m_2\,\omega(c_1 + k_1\tau_1) - \imath k_1\, m_2;\; D_{2\mathrm{g}}(\omega) = D_{11}(\omega). \tag{15}$$

## 2.2 | Non-Dimensionalization

The transfer functions presented in the previous subsection depend on a large number of input variables. Given the complexity of the problem, the application of the Buckingham $\pi$ theorem allows us to define a set of non-dimensional combinations of the design parameters that establish simplified input–output relationships.

In our approach, we used the primary vibration frequency $\omega_1$, the acceleration of gravity $g$ and the primary mass $m_1$ as the basis for non-dimensionalization. This choice offers several advantages as follows:

- the natural frequency $\omega_1$ governs the structure's dynamic response, particularly in relation to resonance phenomena, as well as the frequency ranges where elastic or inertial forces dominate the system's behaviour;
- normalizing with respect to $g$ enables a meaningful comparison of vibration-induced forces with gravitational forces, facilitating generalization across different intensity measures of dynamic input;
- the primary mass $m_1$ captures the inertial properties of the structure, which are critical for scaling the dynamic response.

Thus, we defined the unit length as $[L] = g/\omega_1^2$, the unit mass as $[M] = m_1$ and the unit time as $[T] = \omega_1^{-1}$. Accordingly, for instance, the dynamic stiffness of the vibration absorber reported in Equation (5) could be re-written as follows:

$$k_{\mathrm{d}(\mathrm{SLS})}(\Omega) = \frac{k_{\mathrm{d}}(\omega_1\,\Omega)}{m_1\,\omega_1^2} = \rho_0 + \rho_1\,\frac{\imath\,\bar{\tau}_1\,\Omega}{1 + \imath\,\bar{\tau}_1\,\Omega}, \tag{16}$$

where $i$ is the imaginary unit, $\rho_0 = R_0/\left(m_1\,\omega_1^2\right)$ and $\rho_1 = R_1/\left(m_1\,\omega_1^2\right)$ are the non-dimensional values of the rigidity coefficients in the SLS model; $\bar{\tau}_1 = \omega_1\,\tau_1$ is the non-dimensional relaxation time of the Maxwell element and $\Omega = \omega/\omega_1$ is the non-dimensional frequency of vibration. Similarly to the work by Palmeri and Muscolino on viscoelastically damped foundations [56], the non-dimensional parameters are employed in this study to provide clearer insights into the dynamic behaviour of the SLS-type TMD.

In addition to the commonly used secondary-to-primary mass ratio $\mu = m_2/m_1$ and the equivalent viscous damping ratio of the primary structure $\xi_1 = c_1/(2m_1\omega_1)$, the newly introduced non-dimensional parameters enable a more generalized analysis. These three parameters constitute the minimum number required to fully describe the system while accounting for the physical constraints and interdependencies inherent to the SLS TMD. By framing the problem in a non-dimensionalized form, we ensure that the chosen parameters capture all relevant aspects of the system's dynamic behaviour, while maintaining a clear physical interpretation. This makes the results applicable to various scales, configurations and loading conditions, without the need for design-specific recalibration. Furthermore, these non-dimensional parameters facilitate easier comparisons among different structural solutions, enhancing the assessment of TMD performance across diverse engineering scenarios.



10969845, 2025, 12, Downloaded from https://onlinelibrary.wiley.com/doi/10.1002/eqe.70025 by Uni Federico II Di Napoli, Wiley Online Library on [17/10/2025]. See the Terms and Conditions (https://onlinelibrary.wiley.com/terms-and-conditions) on Wiley Online Library for rules of use; OA articles are governed by the applicable Creative Commons License

## 3 | Optimal Design Parameters for an Undamped Main Structure

### 3.1 | Minimizing RMS Displacements of Undamped Primary Systems Under White Noise

To explore the dynamics of the coupled primary–secondary system and highlight the impact of the viscoelastic device on the structural responses of interest as the design parameters change, sensitivity analyses on the 2-DoF system of Figure 1 were initially performed. The mass ratio $\mu$ was assumed a priori, with $\rho_0$, $\rho_1$ and $\bar{\tau}_1$ treated as the design parameters. In fact, unlike the classical KV-type TMD that involves only two design variables (the tuning and damping ratios), this system considered herein depends on three non-dimensional design parameters.

The results of the sensitivity analyses are shown in Figure 2, where the dynamic amplification factor of the primary mass—defined as the magnitude of the FRF given by either Equation (7) or Equation (12)—is plotted as a function of the dimensionless excitation frequency $\Omega$ for several parametric scenarios.

In all plots, the mass ratio is fixed at $\mu = 0.1$, and the damping of the primary system is neglected ($\xi_1 = 0$). The remaining dimensionless parameters—namely, $\rho_0$, $\rho_1$ and the normalized relaxation time $\bar{\tau}_1$—are varied individually within realistic engineering ranges. Figure 2 reveals that, for both excitation types (i.e., external force $F_1(t)$ and ground acceleration $\ddot{u}g(t)$), the dynamic response amplitude exhibits significant variability, often by several orders of magnitude, even with small changes in these design parameters. This sensitivity strongly emphasizes the need for a robust optimization approach to ensure reliable structural performance.

Interestingly, Figures 2c and 2f show that, as the non-dimensional relaxation time varies within the range $0.005 \leq \bar{\tau}_1 \leq 1$, all plots intersect at the same three points, which are known in the literature as *fixed points* [11, 52]. As discussed by Batou and Adhikari [52], these fixed points form the foundation of the classical $H_\infty$ optimization approach, which is designed to minimize the peak response across the entire frequency spectrum, thereby ensuring robustness. In contrast, $H_2$ optimization seeks to minimize the system's total vibrational energy, focusing on overall performance rather than extreme robustness. However, once damping is introduced into the primary system, these fixed points no longer exist. Therefore, in the remainder of this study, we adopt the $H_2$ optimization strategy, which not only complements existing results for undamped systems but also extends the analysis to a broader range of practical applications where primary damping cannot be disregarded.

Following a similar approach as the one suggested by Asami and Nishihara [48], the two excitations $F_1(t)$ and $\ddot{u}_g(t)$ are modelled as zero-mean Gaussian white noises, with frequency-independent, non-dimensional PSD level $\bar{S}_W$. The root mean square (RMS) of the steady-state displacement of the mass $m_1$ can be calculated as follows (e.g., [57, 58]):

$$\mathbb{E}\left[u_1^2(t)\right] = \left(g/\omega_1^2\right)^2 \bar{S}_W \int_{-\infty}^{+\infty} \left|\bar{H}_{1x(\mathrm{SLS})}(\Omega)\right|^2 \mathrm{d}\Omega\,, \tag{17}$$

in which $\mathbb{E}[\cdot]$ is the expectation operator, while the subscript $x$ of $\bar{H}_{1x}$ refers to either $x = 1$ or $x = g$ depending on the dynamic excitation acting on the system. Furthermore, the overbars on $\bar{S}_W$ and $\bar{H}_{1x}$ indicate their non-dimensional forms. For instance, $\bar{H}_{11}(\Omega) = k_1^{-1} H_{11}(\omega_1\,\Omega)$ for the driving force $F_1(t)$ and $\bar{H}_{1\mathrm{g}}(\Omega) = \omega_1^{-2} H_{1g}(\omega_1\,\Omega)$ for the ground acceleration $\ddot{u}_g(t)$. It is worth highlighting that the optimization procedure proposed in what follows is also applicable to a harmonic signal characterised by a PSD corresponding to a Dirac delta function. This implies that the signal exhibits energy concentrated at a single frequency, resulting in a discrete spectral component. The optimization framework remains valid in this case, as the mathematical formulation and constraints are inherently compatible with signals characterized by such a spectral profile. Substituting Equation (7) into Equation (17), the closed-form expression of the variance of the displacement of the undamped main system subjected to the driving force $F_1(t)$ (i.e., $i = 1$) can be made explicit as follows:

$$\mathbb{E}\left[u_1^2(t)\right] = \frac{\pi\, g^2\, \bar{S}_W}{\mu^2 \rho_1\, \bar{\tau}_1\, \omega_1^4} \Big[\mu(\rho_0 + \rho_1 - 2)(\rho_0 + \rho_1)\bar{\tau}_1^2 + 2\mu(\rho_0 - 1)\rho_0 + \rho_0^2 + \mu^2\left(\bar{\tau}_1^2 + (\rho_0 - 1)\rho_0 + 1\right) + (\rho_0 + \rho_1)^2 \bar{\tau}_1^2\Big] \tag{18}$$

Similarly, in the case of the ground acceleration $\ddot{u}_g(t)$, the RMS particularizes as follows:

$$\mathbb{E}\left[u_1^2(t)\right] = \frac{\pi\, g^2\, \bar{S}_W}{\mu^2 \rho_1\, \bar{\tau}_1\, \omega_1^4} \Big[(\mu+1)^2\rho_0\left(\mu^2 + (\mu+1)^2\rho_0\right) + \mu^2 - 2(\mu+1)^2\mu\rho_0 + \mu^2\bar{\tau}_1^2 + (\mu+1)^3(\rho_0+\rho_1)^2\bar{\tau}_1^2 - 2\mu(\mu+1)(\rho_0+\rho_1)\bar{\tau}_1^2\Big] \tag{19}$$

To optimize the dynamic response of the primary system, the mass ratio $\mu$ was selected as a known parameter, and a minimization procedure was applied to the RMS of the random process $u_1(t)$ with respect to the three design variables as follows: $\rho_0$, $\rho_1$ and $\bar{\tau}_1$. From a mathematical point of view, the considered optimization problem can be formally made explicit as follows:

$$\begin{cases} \min_{\rho_0,\rho_1,\bar{\tau}_1} \mathbb{E}\left[u_1^2\left(\rho_0, \rho_1, \bar{\tau}_1; \mu, \omega_1\right)\right], \\ \text{subject to: } \rho_0 > 0,\ \rho_1 > 0,\ \bar{\tau}_1 > 0, \\ \text{given: } \mu,\ \omega_1,\ \xi_1,\ \bar{S}_W. \end{cases} \tag{20}$$

In the case of an undamped primary structure (i.e., $\xi_1 = 0$), closed-form optimal solutions can be derived. For the sake of clarity, the detailed calculation steps used to analytically obtain Equations (18) and (19) are provided in the Supporting Material: Section 1. Analytical optimal solutions are also summarized in Table 1. It is worth highlighting that Asami and Nishihara [48] have already derived closed-form solutions for an undamped S-DoF oscillator optimally controlled by an SLS-type TMD by, however, adopting a different set of design parameters. In the present paper, by minimizing the RMS of $u_1(t)$ with respect to the dimensionless ratios $\rho_0, \rho_1$ and $\bar{\tau}_1$, we propose optimal formulations that consistently recover the ones provided by Asami et al. [48] when the same set of design parameters is chosen. Therefore, the approach does not represent a fundamentally novel formulation, but rather a generalization that consistently falls into the classical viscously damped case when the relaxation time tends to zero. These compact closed-form expressions



10969845, 2025, 12, Downloaded from https://onlinelibrary.wiley.com/doi/10.1002/eqe.70025 by Uni Federico II Di Napoli, Wiley Online Library on [17/10/2025]. See the Terms and Conditions (https://onlinelibrary.wiley.com/terms-and-conditions) on Wiley Online Library for rules of use; OA articles are governed by the applicable Creative Commons License

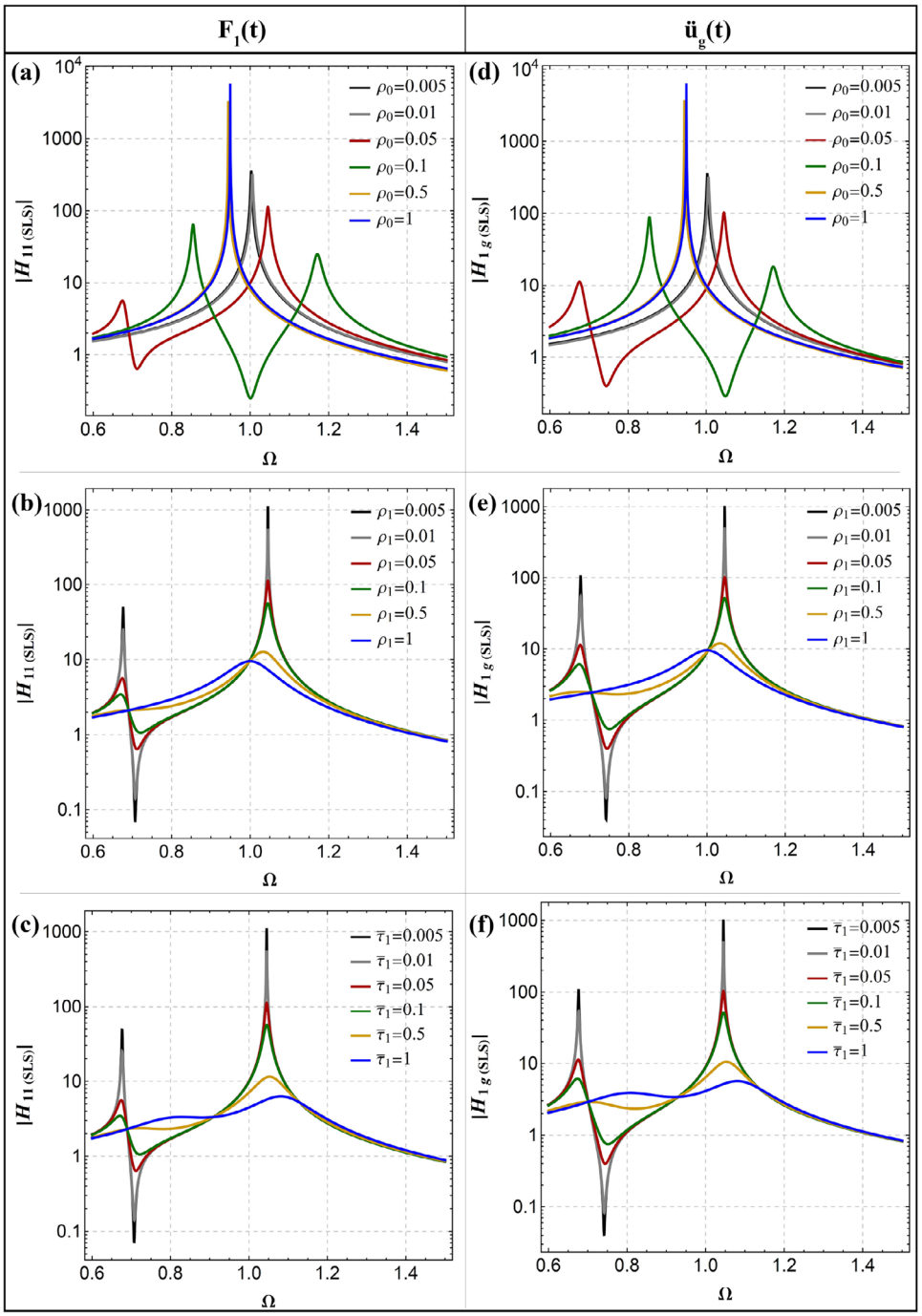


**FIGURE 2** | Sensitivity analyses of SLS-type TMDs: amplification factors of the main system as a function of Ω for the two types of excitation: $F_1$ (a)–(c) and $\ddot{u}_g$ (d)–(f). In all graphics, except when vary, the following non-dimensional parameters are assumed: $\mu = 0.1$, $\xi_1 = 0$, $\rho_0 = 0.05$, $\rho_1 = 0.05$ and $\bar{\tau}_1 = 0.05$.

**TABLE 1** | Closed-form optimal values of the undamped SLS-type TMD for $F_1(t)$ and $\ddot{u}_g(t)$ excitations.

| Excitation type | $\rho_{0,opt}$ | $\rho_{1,opt}$ | $\bar{\tau}_{1,opt}$ |
|---|---|---|---|
| $F_1(t)$ | $\dfrac{\mu\left(1+\mu-\sqrt{\mu(1+\mu)}\right)}{1+\mu}$ | $\dfrac{2\mu^2}{\sqrt{\mu(1+\mu)}}$ | $\sqrt{1+\dfrac{7\mu}{2}+2\mu^2-\dfrac{5+4\mu}{2}\sqrt{\mu(1+\mu)}}$ |
| $\ddot{u}_g(t)$ | $\dfrac{\mu-\mu\sqrt{\mu}}{(1+\mu)^2}$ | $\dfrac{2\mu\sqrt{\mu}}{(1+\mu)^2}$ | $\sqrt{1+\mu-\dfrac{1}{2}(1+\mu)\sqrt{\mu}}$ |



10969845, 2025, 12, Downloaded from https://onlinelibrary.wiley.com/doi/10.1002/eqe.70025 by Uni Federico II Di Napoli, Wiley Online Library on [17/10/2025]. See the Terms and Conditions (https://onlinelibrary.wiley.com/terms-and-conditions) on Wiley Online Library for rules of use; OA articles are governed by the applicable Creative Commons License

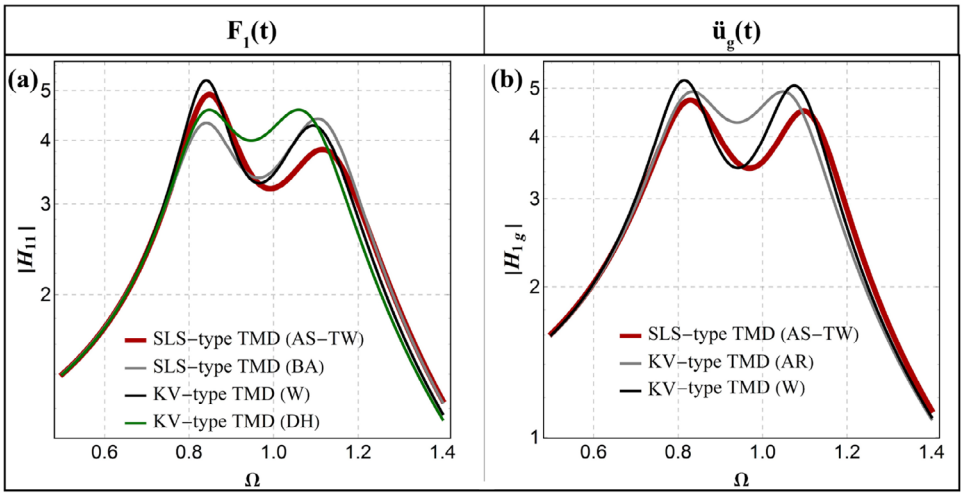


**FIGURE 3** | A comparison of the amplification factors $|H_{11}(\Omega)|$ (a) and $|H_{1g}(\Omega)|$ (b) among optimal KV- and SLS-type TMDs by assuming $\mu = 0.1$ and $\xi_1 = 0$. In plot (a), the curves obtained from the $H_2$ optimization procedures by Asami et al. [48]—this work (AS-TW) and Warburton (W) are compared with the $H_\infty$ ones provided by Batou and Adhikari [52] and Den Hartog [11]. In plot (b), the curves derived by the $H_2$ optimization procedures by Asami et al. [48]—this work (AS-TW) and Warburton (W) are compared with the $H_\infty$ one provided by Argenziano et al. (AR) [59].

serve as an effective and rigorous basis for preliminary design, allowing for the straightforward identification of optimal SLS-TMD parameters under broadband excitation scenarios and for a given mass ratio.

### 3.2 | Comparison Between Optimal SLS- and KV-Type TMD Configurations

To provide insights into the performance of different TMD types (viscously and viscoelastically damped), optimal SLS-type TMDs are compared with optimal KV-type TMDs by applying the optimization procedures proposed in this work and consolidated methods selected from the literature. In Figure 3, the optimal dynamic amplification factors $|H_{11}(\Omega)|$ and $|H_{1g}(\Omega)|$ are plotted as functions of the non-dimensional vibration frequency Ω. The optimal design parameters were calculated using the methods detailed in Refs. [11, 13, 48, 52, 59] and the present study. Two key observations arise as follows: (i) For the SLS-type TMD optimal curves, all procedures yield comparable results regarding vibration amplitude within the relevant frequency range; (ii) compared to the classical KV-type TMD optimal curves, the viscoelastic SLS device, when properly tuned, consistently exhibits enhanced vibration mitigation capabilities for both the driving force $F_1(t)$ and ground acceleration $\ddot{u}_g(t)$. Despite the increased analytical complexity, the additional parameter in the SLS model (i.e., the relaxation time) provides a consistent improvement in the optimization results over the simpler KV model.

## 4 | Optimal Design Parameters for a Damped Main Structure

### 4.1 | Minimizing RMS Displacements of Damped Primary Systems Under White Noise Excitation

Introducing damping into the primary oscillator reduces the overall structural response of the system of Figure 1. While many studies assume zero damping in primary systems of TMD-controlled structures [13, 17, 47, 48, 52], real-world civil engineering structures always exhibit some level of damping. To better capture the actual dynamic behaviour of SLS-type TMDs, a non-zero viscous damping ratio $\xi_1$ was included in the primary system, and sensitivity analyses were conducted to assess its impact on the overall structural response.

From a mathematical perspective, no strict constraints are imposed on the variation of $\xi_1$. However, for practical purposes, the following analyses and the numerical results provided focus on a viscous damping ratio of the primary structure ranging between 0 and 0.10, being 0.10 a limit value that widely includes typical values encountered in civil engineering applications. As shown in Figure 4, even small values of $\xi_1$ significantly affect the dynamic response to both $F_1(t)$ and $\ddot{u}_g(t)$.

Specifically, as well-established, increasing the damping ratio substantially attenuates the resonant peaks of the amplification factors—often by several orders of magnitude—for both considered mass ratio values. From a mechanical perspective, although the influence of the damping parameter $\xi_1$ becomes more pronounced as the mass ratio $\mu$ increases, the amplification factors corresponding to both forced and ground-excited cases at $\mu = 0.5$ remain consistently higher than those at $\mu = 0.05$. In greater detail, comparing the effect of the TMD to that of the primary system's damping ratio reveals that while $\xi_1$ effectively reduces the amplitude of both resonant peaks (with a particularly greater reduction observed in the second peak for $\mu = 0.5$), the mass ratio $\mu$ exerts a stronger influence on the overall frequency response of the system. Specifically, as $\mu$ increases to 0.5, the resonant peaks associated with both $F_1(t)$ and $\ddot{u}g(t)$ responses broaden and their amplitudes grow significantly compared to the low mass ratio case. Across all panels of Figure 4, higher damping ratios (e.g., $\xi_1 = 0.10$) consistently lead to smoother response curves with markedly lower peak amplitudes, thereby confirming that damping plays a critical role over the entire frequency range.



10969845, 2025, 12, Downloaded from https://onlinelibrary.wiley.com/doi/10.1002/eqe.70025 by Uni Federico II Di Napoli, Wiley Online Library on [17/10/2025]. See the Terms and Conditions (https://onlinelibrary.wiley.com/terms-and-conditions) on Wiley Online Library for rules of use; OA articles are governed by the applicable Creative Commons License

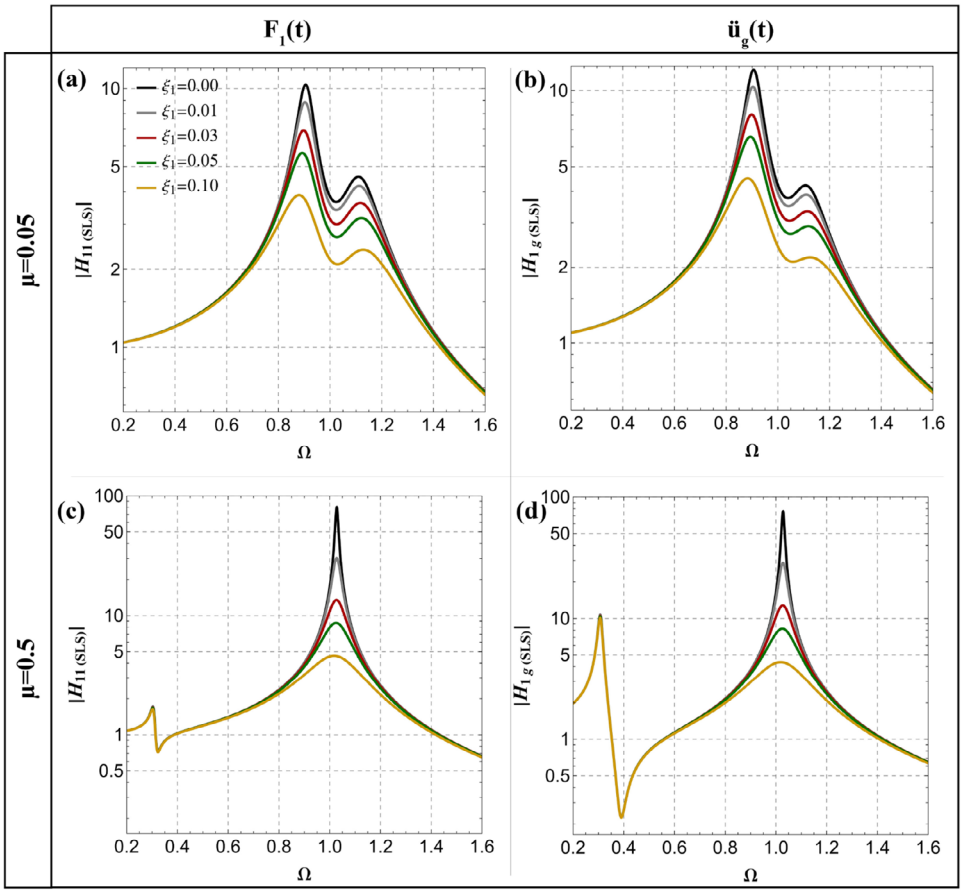


**FIGURE 4** | Plots in logarithmic scale of the amplification factors $|H_{11(\mathrm{SLS})}(\Omega)|$ and $|H_{1g(SLS)}(\Omega)|$ by assuming $\rho_0 = 0.05$, $\rho_1 = 0.1$ and $\bar{\tau}_1 = 0.1$ and by varying $\xi_1$ from 0.00 to 0.10 for two mass ratio values $\mu = 0.05$ and $\mu = 0.5$.

These observations imply that neglecting the damping ratio of the primary structure can result in a substantial overestimation of the system's response, leading to sub-optimal TMD designs.

This sub-section extends our $H_2$ optimization to SLS-type TMDs attached to a damped primary structure. By following the minimization procedure formulated in 20, the same sensitivity analyses from Section 3.1 were repeated by now incorporating the direct impact of the additional non-dimensional parameter $\xi_1$. Results are shown in Figure 5. Specifically, by comparing Figures 2 and 5, the following two key effects are evident: (i) the amplitude of the primary oscillator's response is significantly reduced across the entire frequency range of interest, and (ii) the fixed points independently proposed by Asami and Nishihara [48] and Batou and Adhikari [52] no longer occur in presence of a damped primary structure. Additionally, by observing panels (a) and (d) of Figure 5, one can notice that when $\rho_0$ increases, the resonant peaks tend to converge in a unique one and the amplitude response slightly shifts. With reference to the parameter $\rho_1$, as it increases, the maximum values of the frequency response are drastically decreased and larger values of $\rho_1$ also enhance the energy dissipation, reducing the response amplitude across the whole frequency range and contributing to a smoother curve, while suppressing secondary peaks. Finally, the parameter $\bar{\tau}_1$ governs the relaxation time of the system, therefore, as it increases, the resonance peaks become less sharp and flatter. This behaviour highlights the trade-off between peak suppression and broadening of the frequency response. It is worthing to emphasize that in all subplots of Figure 5, the configuration corresponding to $\rho_0 = \rho_1 = \bar{\tau}_1 = 0.05$ (red curve) exhibits a well-balanced trade-off between peak amplitude suppression and frequency bandwidth, demonstrating almost the same response across both excitation types, while avoiding excessive amplification at off-resonance frequencies.

In order to further investigate the effect of the primary damping $\xi_1$ on the values of the optimal parameters, the variance of the primary structural response $u_1(t)$ was calculated. Explicit expressions of the stationary mean square $\mathbb{E}\left[u_1^2(t)\right]$ were derived following the frequency-based approach proposed by Crandall and Mark [60] as reported in the Supporting Material: Section 1 for both $F_1(t)$ and $\ddot{u}_g(t)$, modelled as zero-mean white noise excitations.

The introduction of the damping parameter $\xi_1$ significantly increases the analytical complexity of the optimization problem compared to previous studies. As a consequence, no closed-form solutions could be obtained for a damped primary structure coupled with an SLS-type TMD, even for the simplest case of broadband inputs. To address this challenge, a numerical minimization procedure was adopted to determine the optimal TMD parameters. To enable this approach, Equation (1) was first reformulated into a convenient state-space representation using the previously defined non-dimensional parameters:



10969945, 2025, 12, Downloaded from https://onlinelibrary.wiley.com/doi/10.1002/eqe.70025 by Uni Federico II Di Napoli, Wiley Online Library on [17/10/2025]. See the Terms and Conditions (https://onlinelibrary.wiley.com/terms-and-conditions) on Wiley Online Library for rules of use; OA articles are governed by the applicable Creative Commons License

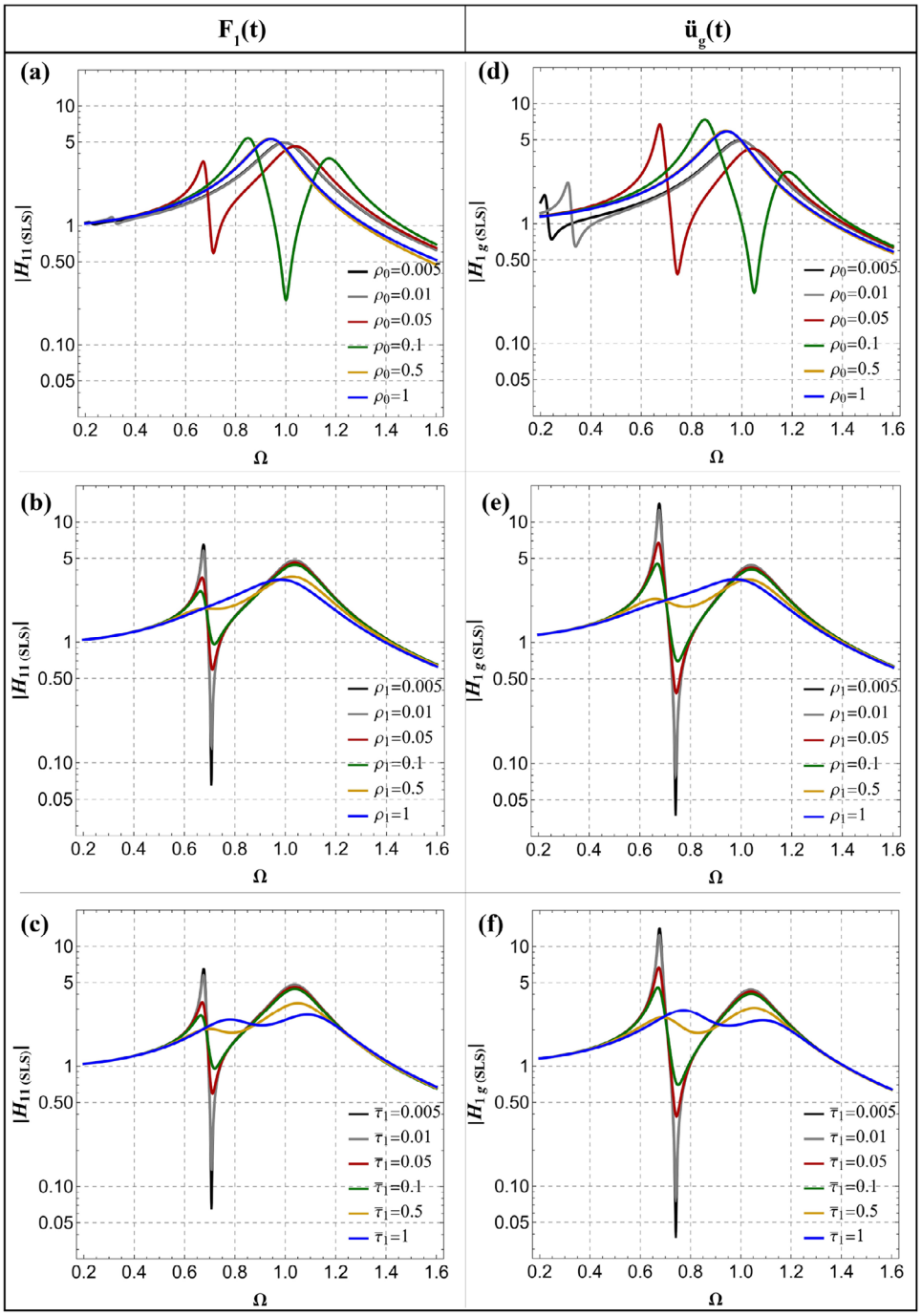


**FIGURE 5** | Sensitivity analysis of the 2-DoF SLS-type TMD system in terms of the amplification factor of the main system as a function of the forced frequency ratio Ω for the two types of excitation: $F_1$ (a)–(c) and $\ddot{u}_g$ (d)–(f). In all graphics, except when vary, the following non-dimensional parameters are assumed: $\mu = 0.1$, $\xi_1 = 0.10$, $\rho_0 = 0.05$, $\rho_1 = 0.05$ and $\bar{\tau}_1 = 0.05$.

$$
\begin{cases}
y_1'(s) = y_3(s) \\
y_2'(s) = y_4(s) \\
y_3'(s) = \rho_1\,\lambda(s) + \rho_0\,y_2(s) - 2\,\xi_1\,y_3(s) - y_1(s) + \bar{F}_1(s) - \bar{a}_g(s) \\
y_4'(s) = y_1(s) + 2\,\xi_1\,y_3(s) - \dfrac{1+\mu}{\mu}(\rho_0\,y_2(s) + \rho_1\,\lambda(s)) - \bar{F}_1(s) \\
\lambda'(s) = y_4(s) - \dfrac{1}{\bar{\tau}_1}\,\lambda(s)
\end{cases}
\tag{21}
$$

where the prime represents differentiation with respect to the non-dimensional time $s = \omega_1\,t$, that is, $(\cdot)' = d(\cdot)/ds$, $y_i(s) = \omega_1^2\,u_i(t)/g$ and $y_{i+2}(s) = \omega_1\,\dot{u}_i(t)/g$ are the non-dimensional displacement and velocity of the mass $m_i$ (with $i = 1, 2$), $g$ being the acceleration of gravity, $\bar{F}_1(s) = F_1(t)/(m_1\,g)$ and $\bar{a}_g(s) = \ddot{u}_g(t)/g$ are the dimensionless dynamic inputs and $\lambda(s)$ is an additional internal variable (AIV) adopted for the linear SLS link [39], representing then non-dimensional deformation of the Maxwell element in the TMD.



10969845, 2025, 12, Downloaded from https://onlinelibrary.wiley.com/doi/10.1002/eqe.70025 by Uni Federico II Di Napoli, Wiley Online Library on [17/10/2025]. See the Terms and Conditions (https://onlinelibrary.wiley.com/terms-and-conditions) on Wiley Online Library for rules of use; OA articles are governed by the applicable Creative Commons License

Let now $\mathbf{y}(s) = \{y_1(s), y_2(s), y_3(s), y_4(s), \lambda(s)\}^\top$ be the time-dependent array collecting the non-dimensional state-space variables that fully characterize the dynamic problem. Equation (21) can then be re-arranged in the following matrix form:

$$\mathbf{y}'(s) = \mathbf{A} \cdot \mathbf{y}(s) + \mathbf{v}\,\bar{W}(s), \tag{22}$$

where $\mathbf{A}$ is the $(5 \times 5)$ matrix of dynamic coefficients, given by the following:

$$\mathbf{A} = \begin{bmatrix} 0 & 0 & 1 & 0 & 0 \\ 0 & 0 & 0 & 1 & 0 \\ -1 & \rho_0 & -2\,\xi_1 & 0 & \rho_1 \\ 1 & -\dfrac{1+\mu}{\mu}\,\rho_0 & 2\,\xi_1 & 0 & -\dfrac{1+\mu}{\mu}\,\rho_1 \\ 0 & 0 & 0 & 1 & -\bar{\tau}_1^{-1} \end{bmatrix}, \tag{23}$$

and $\mathbf{v}$ is the $(5 \times 1)$ load vector, which particularizes as $\mathbf{v} = \{0, 0, 1, -1, 0\}^\top$ for the case of external force and $\mathbf{v} = \{0, 0, -1, 0, 0\}^\top$ for the case of ground acceleration. In both cases, $\bar{W}(s)$ represents the stationary, zero-mean white noise associated with these dynamic inputs.

The stationary mean square vector of the non-dimensional state-space variables can be evaluated as follows (e.g., [57]):

$$\mathbf{m}_{2,\mathrm{y}} = \mathbb{E}[\mathbf{y}(s) \otimes \mathbf{y}(s)] = -2\,\pi\,\bar{S}_W\,\mathbf{A}_2^{-1} \cdot \mathbf{v}_2\,, \tag{24}$$

in which the $(5^2 \times 5^2)$ matrix $\mathbf{A}_2$ and the $(5^2 \times 1)$ vector $\mathbf{v}_2$ are defined as follows:

$$\begin{cases} \mathbf{A}_2 = \mathbf{A} \otimes \mathbf{I}_5 + \mathbf{I}_5 \otimes \mathbf{A} \\ \mathbf{v}_2 = \mathbf{v} \otimes \mathbf{v}, \end{cases} \tag{25}$$

where $\mathbf{I}_5$ is the identity matrix of size 5, and $\otimes$ is the Kronecker product (e.g., [61]). The first component of the $(5^2 \times 1)$ vector $\mathbf{m}_{2,\mathrm{y}}$ is the steady-state variance of the non-dimensional primary displacement $y_1(s)$, that is, $\{\mathbf{m}_{2,\mathrm{y}}\}_1 = \mathbb{E}\left[y_1^2(s)\right]$. The minimization of this quantity with respect to the non-dimensional design parameters $\rho_0$, $\rho_1$ and $\bar{\tau}_1$ represents the objective function of the optimization problem. Within the MATLAB environment [62], both genetic algorithms and particle swarm optimization [63–68] were applied to minimize the target function. In detail, as well-established, both genetic and particle swarm algorithms are susceptible to local minima, which can lead to suboptimal solutions. To overcome this, the algorithm variables are set in order to trace back the optimal parameters' trends of the undamped configuration ($\xi_1 = 0$) for which analytical solutions are available, as reported in Table 1. This strategy ensures that the global optimum is correctly identified also for slightly damped primary systems ($\xi_1$ up to 0.10). Figures 6 and 7 show the results of the proposed optimization strategy, respectively, for the forced excitation $F_1(t) = W(t)$ and the ground acceleration $\ddot{u}_{\mathrm{g}}(t) = W(t)$.

To assess the effectiveness of the approach, a non-dimensional performance index $PI$ is introduced, that is,

$$PI = \frac{\mathbb{E}\left[y_{1,opt}^2(t)\right]}{\pi\,\bar{S}_W/(2\,\xi_1)}, \tag{26}$$

that is the ratio between the RMS of $y_1(s)$ for the optimal TMDs and that of an uncontrolled S-DoF system. In Figures 6a and 7a, this index $PI$ is plotted as a function of the mass ratio $\mu$, with the equivalent viscous damping ratio $\xi_1$ varying between 0.00 and 0.10. It can be observed that, for mass ratios $\mu$ between 0 and 0.4, a relatively low damping in the primary oscillator leads to a significant reduction in the non-dimensional variance (proportional to $PI$), that decreases monotonically as the mass ratio $\mu$ increases for all values of damping, being instead the effect of $\xi_1$ less pronounced for large mass ratios. For both excitation cases, when $\xi_1 = 0$, the performance index $PI$ vanishes (Figures 6a and 7a), while the optimal parameters design parameters (Figures 6b–d and 7b–d) exactly match the analytical solutions (Table 1) derived for the undamped system and somehow existing in the inherent literature [48].

Additionally, while the optimal parameters $\rho_{0,\mathrm{opt}}$, $\rho_{1,\mathrm{opt}}$ and $\bar{\tau}_{1,\mathrm{opt}}$ exhibit minimal sensitivity to variations in $\xi_1$ under forced excitation (see Figure 6b–d), the damping ratio plays a significantly more prominent role in the case of ground motion excitation (see Figure 7b–d). In this context, structural damping affects how effectively the system transmits the frequency content of the ground acceleration to both the primary and secondary masses, thereby enhancing overall energy dissipation.

Overall, the findings indicate that assuming zero damping in the primary system can lead to significant inaccuracies in determining the optimal TMD parameters, even for low primary viscous damping ratios ($\xi_1 \leq 0.10$). Therefore, the optimal parameters, presented graphically as functions of the mass ratio $\mu$ (see Figures 6 and 7), should be used for the initial design of SLS-type TMDs, especially when the dynamic input can be considered a broadband excitation. It is worth again highlighting that, although the results refer to some values of mass ratios and damping of the primary system limited to ranges of interest for civil engineering applications, the proposed strategy can be readily generalised to any value of $\mu$ and $\xi_1$.

## 4.2 | Comparison Between Optimal SLS- and KV-Type TMD Configurations

### 4.2.1 | Frequency Response and Expected Displacement Values of Primary Masses for SLS- and KV-Type TMD Systems

The comparison between SLS- and KV-type TMDs, discussed in Section 3.2, is revisited here by accounting for the effect of viscous damping in the primary structure on optimal configurations. In Figure 8, the optimal amplification factors of the main system are plotted for both excitation types, $F_1(t)$ and $\ddot{u}_{\mathrm{g}}(t)$. By assuming mass ratio $\mu = 0.1$ and viscous damping ratio $\xi_1 = 0.05$, the optimal configurations of KV-type TMDs are determined using $H_\infty$ and $H_2$ optimization procedures from Ref. [59]:

- $\nu_{opt} = 0.9047$ and $\xi_{2,opt} = 0.1935$ for the forced case;
- $\nu_{opt} = 0.8769$ and $\xi_{2,opt} = 0.2097$ for the ground acceleration case;



10969845, 2025, 12, Downloaded from https://onlinelibrary.wiley.com/doi/10.1002/eqe.70025 by Uni Federico II Di Napoli, Wiley Online Library on [17/10/2025]. See the Terms and Conditions (https://onlinelibrary.wiley.com/terms-and-conditions) on Wiley Online Library for rules of use; OA articles are governed by the applicable Creative Commons License

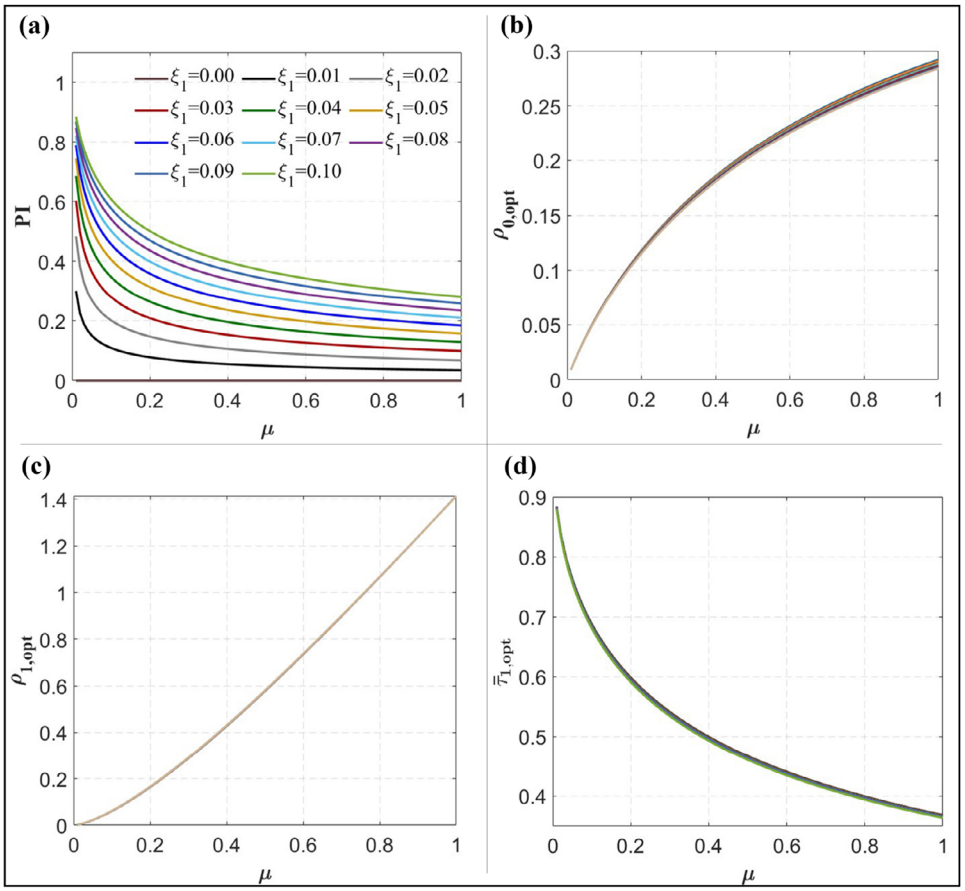


**FIGURE 6** | Optimal parameters of SLS-type TMDs as a function of $\mu$ with $\xi_1$ varying from 0.00 to 0.10, by assuming a white noise excitation acting as $F_1(t)$ on the main mass: (a) optimal non-dimensional variance *PI*; (b) optimal $\rho_0$; (c) optimal $\rho_1$ and (d) optimal $\bar{\tau}_1$. Since the *PI* index has been evaluated directly proportional to $\xi_1$, it is constantly zero in plot (a) for null damping in the main structure. However, when $\xi_1 = 0$, the optimal design parameters perfectly recover the optimal trend, whose analytical formulations are provided in Table 1 for the forced case.

the coefficients $\nu_{opt}$ and $\xi_{2,opt}$, respectively, denoting the optimal frequency ratio $\omega_2/\omega_1$ and the damping ratio of the secondary system.

Moreover, the optimal SLS-type TMDs follow the method introduced in Section 4.1. For instance, by selecting the same input parameters of the previous case, the optimal design parameters $\rho_{0,\text{opt}}$, $\rho_{1,\text{opt}}$ and $\bar{\tau}_{1,\text{opt}}$ are as follows:

- 0.0691, 0.0609 and 0.6847 for the forced case;
- 0.0494, 0.0498 and 1.0728 for the ground acceleration case.

From the direct comparison of Figures 3 and 8, the following two key observations arise: (i) Introducing non-zero damping in the primary structure reduces the overall amplitude response in both loading cases, and (ii) as in the undamped case, the optimally tuned viscoelastically damped TMD consistently outperforms the classical KV-type TMD in reducing the dynamic response. Further details on the comparison between KV- and SLS-type TMDs in terms of the *PI* parameter have been reported in Section 2 of the Supporting Material, where the expected displacement values of both configurations normalized with respect to the one of the non-controlled (NC) structure are represented in Figure S1.

#### 4.2.2 | Time History Analyses on Lumped Mass Models Subjected to Natural Seismic Accelerograms

In order to assess the findings of the optimization procedure on damped main structures, a set of seven natural accelerograms (see Table S3 in the Supporting Material) has been selected for providing more specific case studies and realistic comparisons. In particular, explicit dynamic time history analyses have been carried out on lumped mass models within the finite element environment SAP2000 [69], by comparing NC structures with optimal KV- and SLS-type TMD configurations (as schematically illustrated in Figure 9a). More in detail, for the numerical simulations, the data of the primary mass—modelled as a single unidirectional DoF—are derived from the tall building case study reported in [9], here recalled:

- $m_1 = 8.7 \times 10^7$ kg, $k_1 = 1.305 \times 10^{10}$ N m$^{-1}$ and $c_1 = 3.37 \times 10^7$ N s m$^{-1}$.

By adopting the optimal KV- and SLS-type TMD configurations for the ground acceleration case reported in previous Subsection 4.2 and still assuming $\mu = 0.1$ and $\xi_1 = 0.05$, the following mechanical parameters are obtained for the secondary mass:

- $m_2 = 8.7 \times 10^6$ kg for both KV- and SLS-type TMDs;



10969845, 2025, 12, Downloaded from https://onlinelibrary.wiley.com/doi/10.1002/eqe.70025 by Uni Federico II Di Napoli, Wiley Online Library on [17/10/2025]. See the Terms and Conditions (https://onlinelibrary.wiley.com/terms-and-conditions) on Wiley Online Library for rules of use; OA articles are governed by the applicable Creative Commons License

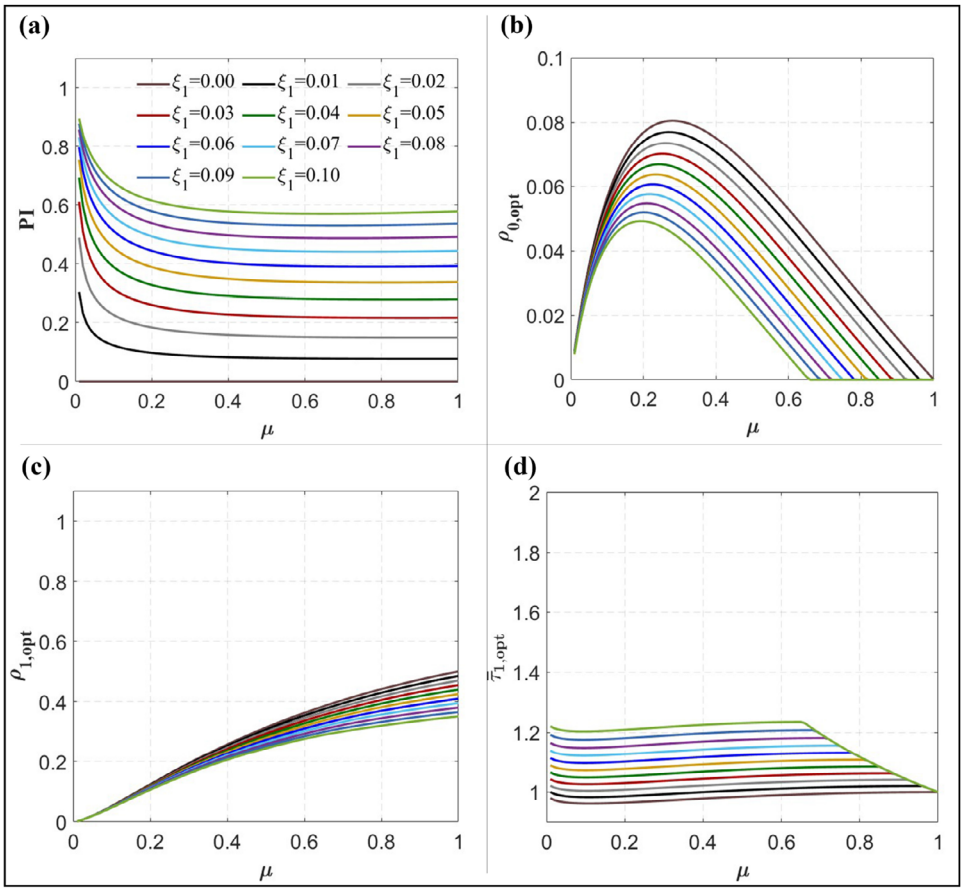


**FIGURE 7** | Optimal parameters of SLS-type TMDs as a function of $\mu$ with $\xi_1$ varying from 0.00 to 0.10, by assuming a ground motion acceleration $\ddot{u}_g$ modelled as a white noise input: (a) optimal non-dimensional variance $PI$; (b) optimal $\rho_0$; (c) optimal $\rho_1$ and (d) optimal $\bar{\tau}_1$. Also in this case, the $PI$ index assumes the zero value in plot (a), when $\xi_1 = 0$. In this case, the optimal design parameters perfectly recover the optimal trend, whose analytical formulations are provided in Table 1 for the ground motion excitation.

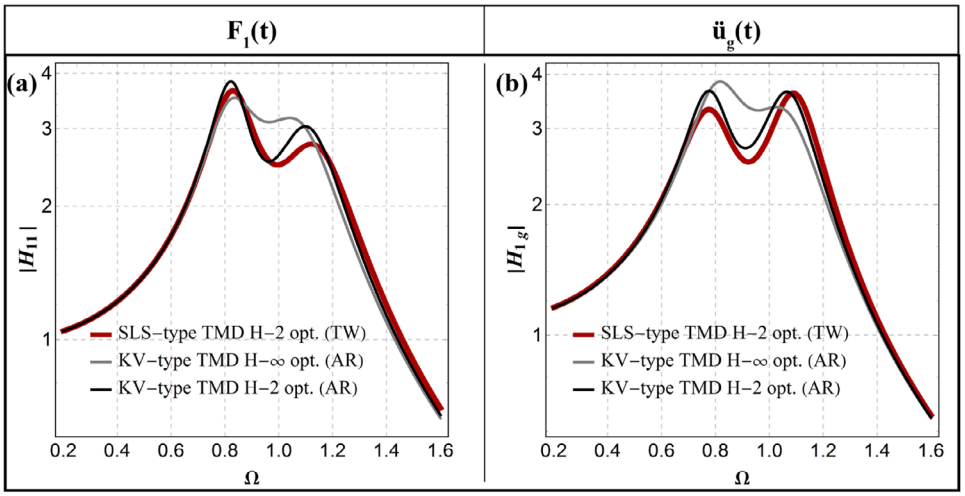


**FIGURE 8** | Comparison between KV- and SLS-type optimal configurations. In plots (a) and (b), the amplification factors $|H_{11}(\Omega)|$ (a) and $|H_{1g}(\Omega)|$ obtained from $H_\infty$ and $H_2$ optimization procedures of KV-type TMDs by Argenziano et al. [59] (AR) are compared to the ones derived for the $H_2$ optimization for SLS-type TMDs proposed in this work (TW), by assuming $\mu = 0.1$ and $\xi_1 = 0.05$.



10969945, 2025, 12, Downloaded from https://onlinelibrary.wiley.com/doi/10.1002/eqe.70025 by Uni Federico II Di Napoli, Wiley Online Library on [17/10/2025]. See the Terms and Conditions (https://onlinelibrary.wiley.com/terms-and-conditions) on Wiley Online Library for rules of use; OA articles are governed by the applicable Creative Commons License

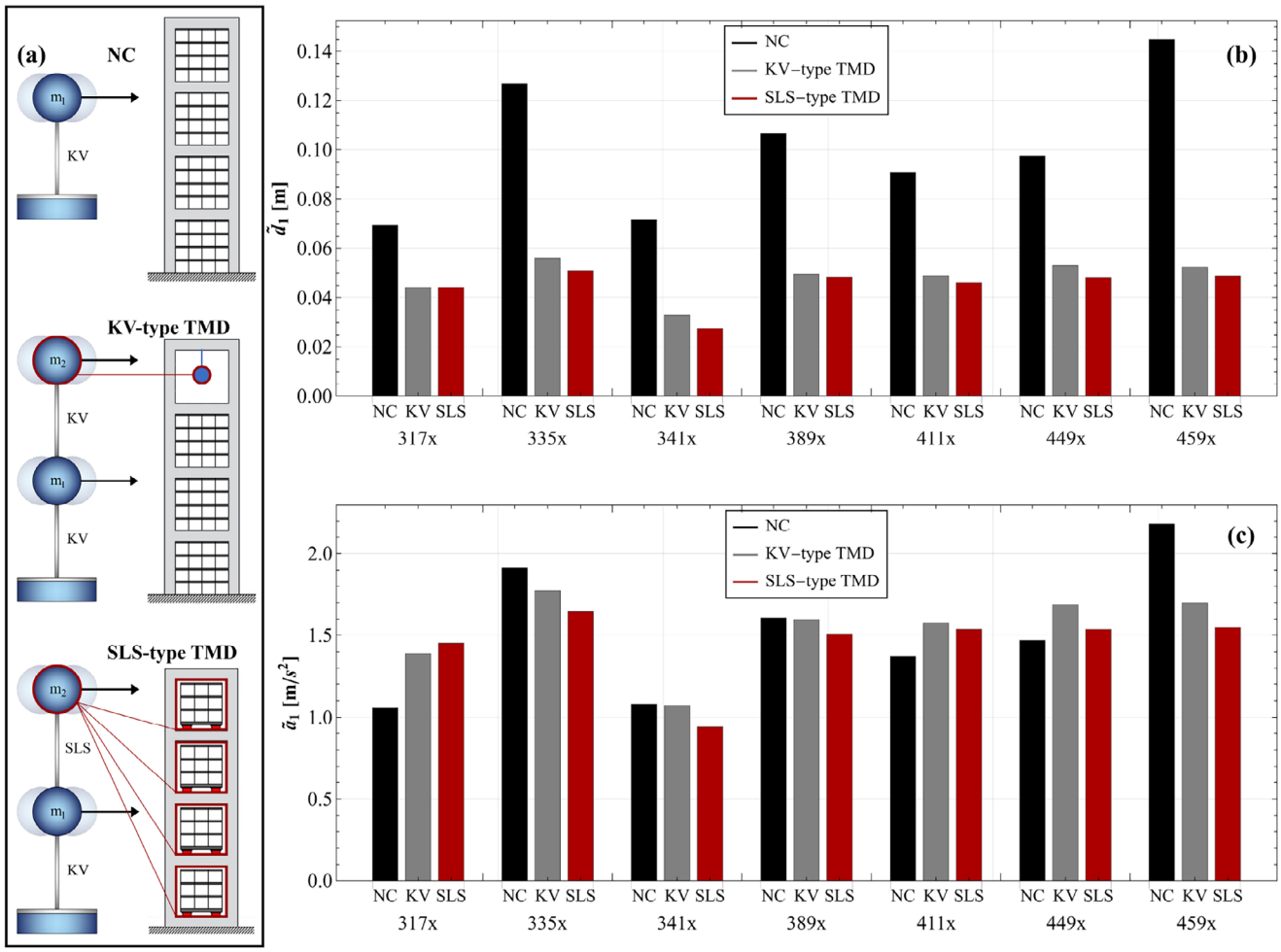


**FIGURE 9** | Comparison among the dynamic response of the three lumped mass systems (damping ratio $\xi_1 = 0.05$) depicted in part (a): maximum peak displacements $\tilde{d}_1$ (b) and peak accelerations $\tilde{a}_1$ (c), resulting from the time history analyses with the set of seven accelerograms carried out on lumped mass systems, that is, non-controlled structure (NC), KV- and SLS-type optimal TMD configurations. In part (a), it is emphasized that KV model can be adopted for conventional TMDs, while, when isolation bearings or other viscoelastic devices are employed for disconnecting primary and absorber mass/masses, the SLS model can be more suitable, also by still considering a reduced-order 2-DoFs system for the several absorber masses (i.e., $m_2$) and the main structure (i.e., $m_1$).

- $k_{2,\text{opt}} = 1.003 \times 10^5$ N m$^{-1}$ for the KV-type system and $R_{0,\text{opt}} = 6.446 \times 10^7$ N m$^{-1}$ and $R_{1,opt} = 6.498 \times 10^7$ N m$^{-1}$ for the SLS-type TMD;
- $c_{2,\text{opt}} = 1.2398 \times 10^7$ N s m$^{-1}$ for the KV-type configuration and $c_{0,\text{opt}} = 1.801 \times 10^7$ N s m$^{-1}$ for the SLS-type one.

The results of the analyses are reported in terms of maximum peak displacements and acceleration of the main mass, respectively, indicated with $\tilde{d}_1$ and $\tilde{a}_1$. From the chart of Figure 9a, one can notice that the maximum peak displacements $\tilde{d}_1$ are higher for the NC structure compared to the KV- and SLS-type TMDs across all the earthquake excitations. Additionally, the SLS-type system achieves greater displacement reduction compared to the KV-type TMD, with the sole exception of the signal ID 317x where peaks appear practically analogous. For the selected set of natural accelerograms, the SLS system shows particular effectiveness in the case of the seismic event 341x, where peak displacement reductions of 63% and 17% are obtained, respectively, with respect to the NC and the KV-type configurations. Unlike displacements, the reduction in accelerations $\tilde{a}_1$ is more balanced between KV- and SLS-type TMD, where higher acceleration values are displayed for some seismic signals with respect to NC configurations. However, this can be attributed to the increase in the total mass of the KV- or SLS-type TMD system compared to that one of the uncontrolled configuration, as an additional mass equivalent to 10% of the primary mass is introduced. While this results into an overall reduction of $\tilde{d}_1$, it may still lead to increased accelerations in the primary system for certain seismic events, although the SLS-type TMD almost always achieves lower acceleration values with respect to the KV-type counterpart.

With the aim of validating the proposed approach, further results of time history analyses are provided for a representative earthquake event, ID 341x (see Table S3 of the Supporting Material). In particular, Figure 12a reproduces the ID 341x ground acceleration input ($\ddot{u}_g$), while the displacement history of the primary system, that is, $d_1$, has been evaluated for the NC structure, KV-type TMD and SLS-type TMD configurations in Figure 12b, with a focus on the time interval 16–20 s (see Figure 12b). From the figure, one



10969845, 2025, 12, Downloaded from https://onlinelibrary.wiley.com/doi/10.1002/eqe.70025 by Uni Federico II Di Napoli, Wiley Online Library on [17/10/2025]. See the Terms and Conditions (https://onlinelibrary.wiley.com/terms-and-conditions) on Wiley Online Library for rules of use; OA articles are governed by the applicable Creative Commons License

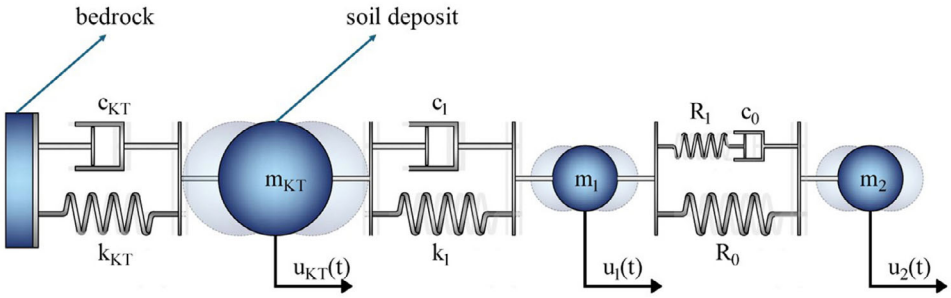


**FIGURE 10** | Structural 2-DoF SLS-type TMD model equipped with the KT filter, being $c_{KT}$ and $k_{KT}$, respectively, the damping factor and the stiffness of the KT oscillator.

can observe that the SLS-type TMD almost always performs better than the KV-type counterpart, with displacement reduction of more than 15% in several time instants. For more details and in-depth discussion of these results, see the corresponding paragraph of Section 2 of the Supporting Material, where further findings are displayed in Figure S2.

## 4.3 | Minimum RMS of the Displacement of the Damped Primary System Under Coloured Excitation

### 4.3.1 | Extension to Non-Uniform PSD Earthquake Inputs

In the previous sections, the optimization of SLS-type TMDs was carried out by making reference to both excitations $F_1(t)$ and $\ddot{u}_g(t)$ as modelled as white noise inputs. However, it is widely known that earthquake ground motions cannot realistically be considered as realization of a white noise, as their PSD is not uniform across the frequency range of interest. To more accurately investigate the effects of coloured excitations on the optimal design of SLS-type TMDs, we here further extend the proposed theoretical strategy by considering the additional presence of a filter capable of capturing realistic seismic inputs. Without loss of generality, we here make reference to the KT filter, widely employed in the modelling of earthquake ground accelerations [70, 71]. As well known, the KT model represents the soil deposit over the bedrock as a linear oscillator, which is subjected to a Gaussian white noise process during seismic events (see Figure 10). Specifically, the mass $m_{KT}$ of the KT oscillator is assumed to be infinite (i.e., much larger than that of the superstructure), while its damping ratio $\xi_{KT}$ and natural circular frequency $\omega_{KT}$ are calibrated based on historical ground motion records. The seismic acceleration produced by the KT filter can be expressed as follows:

$$\ddot{u}_g(t) = -\omega_{KT}^2\, u_{KT}(t) - 2\,\xi_{KT}\,\omega_{KT}\,\dot{u}_{KT}(t)\,, \tag{27}$$

where $u_{KT}(t)$ and $\dot{u}_{KT}(t)$ represent the displacement and velocity of the KT oscillator relative to the bedrock, respectively. Furthermore, the PSD of the seismic acceleration $\ddot{u}_g(t)$ at the base of the structure is given by the following:

$$S_{\ddot{u}_g}(\omega) = \frac{\omega_{KT}^4 + 4\,\xi_{KT}^2\,\omega_{KT}^2\,\omega^2}{\left(\omega_{KT}^2 - \omega^2\right)^2 + 4\,\xi_{KT}^2\,\omega_{KT}^2\,\omega^2}\, S_W \tag{28}$$

where $S_W$ is the PSD of the Gaussian white noise acting at the bedrock. In terms of non-dimensional state-space variables, the filter equations can be expressed as follows:

$$\begin{cases} z_2'(s) = -\Omega_{KT}^2\, z_1(s) - 2\,\xi_{KT}\,\Omega_{KT}\, z_2(s) - \bar{W}(s) \\ \ddot{u}_g(t) = g\, a_g(s) = -g\left[\Omega_{KT}^2\, z_1(s) + 2\,\xi_{KT}\,\Omega_{KT}\, z_2(s)\right] \end{cases} \tag{29}$$

where $u_{KT}(t) = g\, z_1(s)/\omega_1^2$, $\dot{u}_{KT}(t) = g\, z_2(s)/\omega_1$ and $\Omega_{KT} = \omega_{KT}/\omega_1$.

The adoption of the KT filter results in an enlarged state-space model. Equation (22) is still valid, but the array collecting the non-dimensional state variable is now $(7\times 1)$ and can be block-partitioned as $\mathbf{y}(s) = \{y_1(s), y_2(s), y_3(s), y_4(s), \lambda(s) \mid z_1(s), z_2(s)\}^\top$, where the first five state variables are those of the primary and secondary masses (i.e., the same as in Sub-section 4.1) and the additional two state variables are associated with the KT filter. Similarly, the $(7\times 7)$ matrix of dynamic coefficients can be block-partitioned:

$$\mathbf{A} = \left[\begin{array}{ccccc|cc} 0 & 0 & 1 & 0 & 0 & 0 & 0 \\ 0 & 0 & 0 & 1 & 0 & 0 & 0 \\ -1 & \rho_0 & -2\,\xi_1 & 0 & \rho_1 & \Omega_{KT}^2 & 2\,\xi_{KT}\,\Omega_{KT} \\ 1 & -\dfrac{1+\mu}{\mu}\,\rho_0 & 2\,\xi_1 & 0 & -\dfrac{1+\mu}{\mu}\,\rho_1 & 0 & 0 \\ 0 & 0 & 0 & 1 & -\bar{\tau}_1^{-1} & 0 & 0 \\ \hline 0 & 0 & 0 & 0 & 0 & 0 & 1 \\ 0 & 0 & 0 & 0 & 0 & -\Omega_{KT}^2 & -2\,\xi_{KT}\,\Omega_{KT} \end{array}\right], \tag{30}$$

and the same can be done for the $(7\times 1)$ load vector, which particularizes as $\mathbf{v} = \{0, 0, 0, 0, 0 \mid 0, -1\}^\top$.

As the mathematical structure of the problem remains unchanged (only its dimensionality has increased), the variance of the target seismic response $u_1(t)$ can still be calculated using the procedure outlined in Sub-section 4.1; that is, $\mathbb{E}[u_1^2(t)] = (g/\omega_1^2)^2\,\mathbb{E}[y_1^2(s)] = (g/\omega_1^2)^2\,\{\mathbf{m}_{2,y}\}_1$. Under the filtered white noise, the array $\{\mathbf{m}_{2,y}\}$ is still given by Equation (24), but this time its dimensions are $(7^2\times 1)$.

The optimization procedures detailed in Sub-section 4.1 were re-applied to design optimal SLS-type TMDs under coloured (rather than white) excitation. Three different values were assumed for



10969845, 2025, 12, Downloaded from https://onlinelibrary.wiley.com/doi/10.1002/eqe.70025 by Uni Federico II Di Napoli, Wiley Online Library on [17/10/2025]. See the Terms and Conditions (https://onlinelibrary.wiley.com/terms-and-conditions) on Wiley Online Library for rules of use; OA articles are governed by the applicable Creative Commons License

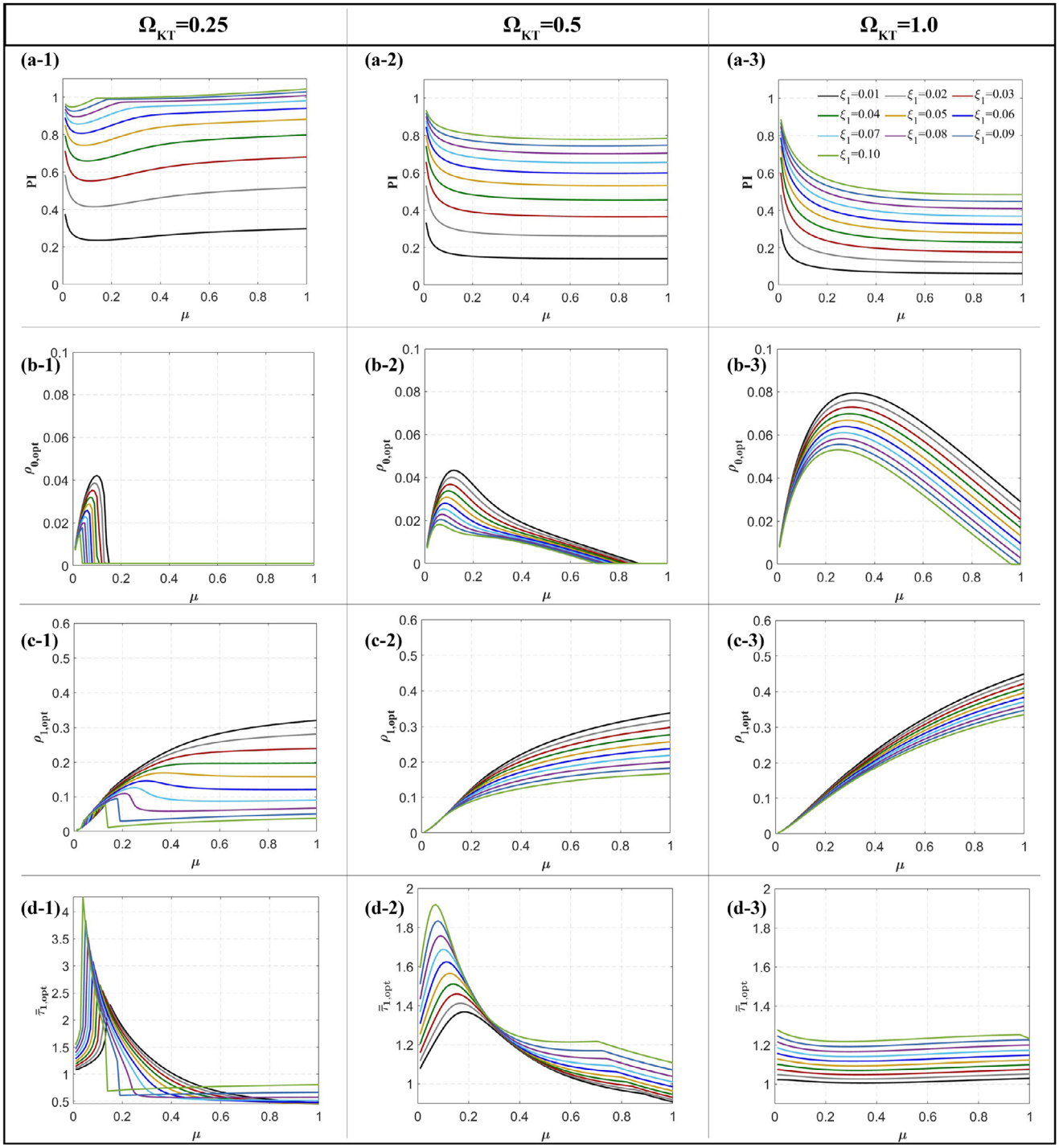


**FIGURE 11** | Optimal parameters of SLS-type TMDs as a function of $\mu$ with $\xi_1$ varying from 0.01 to 0.10, $\xi_{KT} = 0.6$ and by employing a KT filter with $\Omega_{KT,i} = 0.25, 0.5, 1$: (a-1) optimal non-dimensional variance $PI$; (b-1) optimal $\rho_0$; (c-1) optimal $\rho_1$ and (d-1) optimal $\bar{\tau}_1$.

the undamped natural frequency of the KT filter, namely $\Omega_{KT} = 0.25, 0.5, 1$, with the equivalent viscous damping ratio of the KT oscillator set to $\xi_{KT} = 0.6$. The resulting optimal design parameters are displayed in Figure 11, as a function of the mass ratio $\mu$ and for several values of the primary viscous damping ratio $\xi_1$.

A comparison of the optimization results for filtered (Figure 11a) versus unfiltered (Figure 7) white noise ground motion reveals notable trends:

- For $\Omega_{KT} = 1$, the white noise excitation is filtered by a soil deposit with dynamic properties similar to those of the main structure. Consequently, the optimal TMD parameters closely resemble those derived for direct white noise excitation. Significant deviations in the optimal values of $\rho_0$ and $\bar{\tau}_1$ only occur for relatively high mass ratios.
- For $\Omega_{KT} = 0.25$ and $\Omega_{KT} = 0.5$, larger deviations in the optimal parameters are observed, indicating that the system's



10969845, 2025, 12, Downloaded from https://onlinelibrary.wiley.com/doi/10.1002/eqe.70025 by Uni Federico II Di Napoli, Wiley Online Library on [17/10/2025]. See the Terms and Conditions (https://onlinelibrary.wiley.com/terms-and-conditions) on Wiley Online Library for rules of use; OA articles are governed by the applicable Creative Commons License

optimum strongly depends on the frequency content of the non-uniform PSD input. Interestingly, Figure 11 shows a reduction in the non-dimensional optimal equilibrium modulus $\rho_{0,\text{opt}}$ in the KT case. In the low-to-moderate mass ratio range, this reduction in the absorber's elastic stiffness is compensated by an increase in the optimal non-dimensional relaxation time $\bar{\tau}_{1,\text{opt}}$, implying that the primary-to-secondary mass link becomes 'less viscous' and 'more elastic' than in the white noise case.

- Finally, for $\Omega_{KT} = 0.25$, the performance indicator $PI$ tends to become larger than one for large mass ratios and for primary damping ratios $\xi_1 > 0.07$. This suggests that, for such specific combinations of parameters, the effectiveness of the viscoelastic vibration absorber diminishes, thus limiting the benefits of tuning the TMD.

With respect to the rows, further comments can be made:

- Row (a): Optimal non-dimensional variance ($PI$) (a-1), (a-2) and (a-3) show how this parameter evolves for different $\Omega_{KT}$ values. For lower $\Omega_{KT}$ (e.g., 0.25), $PI$ demonstrates less variation as $\mu$ increases. As $\Omega_{KT}$ rises to 1.0, the curves show a more significant decrease with increasing $\mu$, reflecting enhanced performance at higher mass ratios;
- Row (b): These plots represent the variation of optimal $\rho_0$ at different $\Omega_{KT}$, by varying the damping ratio. For all $\Omega_{KT}$ values, $\rho_0$ initially rises to a peak and then tapers off as $\mu$ increases. The peak shifts slightly with increasing $\Omega_{KT}$, indicating a dependence on this frequency ratio parameter;
- Row (c): The optimal parameter $\rho_1$, related to tuning, grows steadily with $\mu$. This trend is consistent across all values of $\Omega_{KT}$, but the growth rate becomes more pronounced at higher $\Omega_{KT}$;
- Row (d): Optimal $\bar{\tau}_1$ exhibits a decaying trend for all cases. The decay is steepest for the smallest $\Omega_{KT}$ and becomes more gradual as $\Omega_{KT}$ increases, suggesting that the time-dependent characteristics of the TMD are more stable at higher frequency ratios.

#### 4.3.2 | Comparison Between Sub-Optimal and Optimal Configurations Subjected to Coloured Excitations

To demonstrate the effectiveness of the proposed methodology and emphasize the critical importance of designing TMD systems based on the frequency content of earthquake inputs, time history analyses have been conducted considering the Hyogo-Ken Nanbu earthquake (ID 411x, see Table S3 of the Supporting Material) and a comparison between sub-optimal and optimal TMD configurations is here provided. To do this, the following set of parameters is considered for the main mass:

- $m_1 = 8.7 \times 10^7$ kg, $k_1 = 5.0184 \times 10^{10}$ N m$^{-1}$ and $c_1 = 2.0910 \times 10^8$ N s m$^{-1}$;

The equivalent KT filter parameters for the accelerogram ID 411x are given as $S_W = 0.25$ m$^2$ s, $\omega_{KT} = 12$ rad s$^{-1}$ and $\xi_{KT} = 0.3$ [72, 73], thus obtaining $\Omega_{KT} \simeq 0.5$.

By assuming mass ratio $\mu = 0.1$ and $\xi_1 = 0.05$, the parameters of the absorber mass of the KV-type TMD resulting from the $H_\infty$ optimization procedure given by Argenziano et al. [59] are estimated as follows:

- $m_2 = 8.7 \times 10^6$ kg, $k_{2,\text{opt}} = 3.8587 \times 10^9$ N m$^{-1}$ and $c_{2,\text{opt}} = 7.6889 \times 10^7$ N s m$^{-1}$;

Then, implementing the optimization procedure of the SLS-type TMDs for both the two modelling strategies of the input, that is, the white noise and the KT earthquake excitation, two different sets of optimal parameters can be obtained by assuming the same mass $m_2$ and particularise as follows:

- $R_{0,\text{opt-WN}} = 2.4791 \times 10^9$ N m$^{-1}$, $R_{1,\text{opt-WN}} = 2.4992 \times 10^9$ N m$^{-1}$ and $c_{0,\text{opt-WN}} = 1.1171 \times 10^8$ N s m$^{-1}$;
- $R_{0,\text{opt-KT}} = 7.5277 \times 10^7$ N m$^{-1}$, $R_{1,\text{opt-KT}} = 3.387 \times 10^9$ N m$^{-1}$ and $c_{0,\text{opt-KT}} = 2.656 \times 10^8$ N s m$^{-1}$;

where the subscripts WN and KT, respectively, refer to the white noise and the KT filtered model.

The comparative analysis of the structural responses for the KV-type TMD, the SLS-type TMD optimized with a white noise (WN) filter and the SLS-type TMD optimized with a KT filter (subjected to accelerogram ID 411x) is illustrated in Figure 12. In detail, plot of Figure 12c displays the input ground acceleration ID 411x, while plots (d) and (e) present the corresponding displacement responses of the primary system.

The results reveal that both SLS-type TMD configurations outperform the KV-type TMD in mitigating displacements, with the SLS-KT filter showing a slightly better response reduction compared to the SLS-WN filter. Higher performance of the SLS configurations is particularly evident in Figure 12e, where a zoomed-in view emphasizes how oscillation amplitudes are consistently lower in the SLS-KT system. By comparing the peak responses, the scatter between SLS-WN and SLS-KT configurations can be greater than 20%, while the difference with respect to the conventional KV-type TMDs values can even overcome the 25%. In particular, a larger overview of these results is reproduced also in Figure S3 of Section 2 of the Supporting Material.

Therefore, these observations confirm how the use of KT filter further enhances the performance of the SLS-TMD by more effectively accounting for the actual seismic frequency content.

It is important to note that the optimization procedure in this study was conducted entirely within the linear elastic domain, as is common in preliminary and pre-sizing design stages of TMD devices. However, in some cases, real structures may exhibit significant non-linear behaviours, especially during severe seismic events, including, for instance, constitutive non-linearities, such as stiffness degradation, material yielding and geometric non-linearities due to large displacements. To investigate these effects, additional time-history analyses were performed using lumped mass models with a Pivot-type non-linear constitutive law to simulate damage-induced stiffness degradation, as detailed in Section 2 of the Supporting Material. Results demonstrate that, even within the non-linear framework, TMD-equipped sys-



10969845, 2025, 12, Downloaded from https://onlinelibrary.wiley.com/doi/10.1002/eqe.70025 by Uni Federico II Di Napoli, Wiley Online Library on [17/10/2025]. See the Terms and Conditions (https://onlinelibrary.wiley.com/terms-and-conditions) on Wiley Online Library for rules of use; OA articles are governed by the applicable Creative Commons License

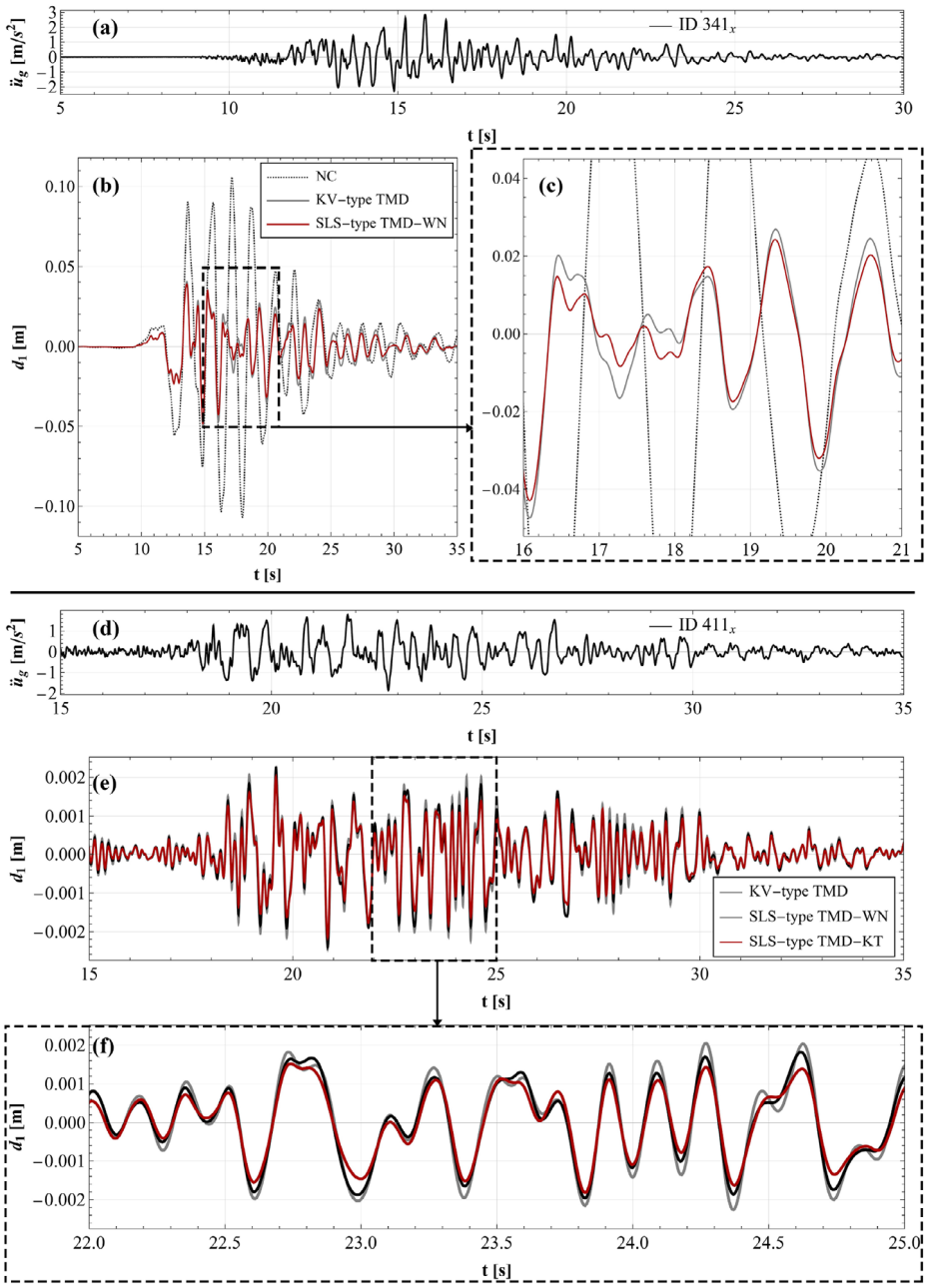


**FIGURE 12** | Results of the time-history analyses in terms of displacements ($d_1$) of the primary systems. In plot (a) and (d), the selected accelerogram input, respectively, ID 341x and 411x, are provided. In detail, plot (b) and its corresponding inset, plot (c), reproduce the comparison among non-controlled structure (NC), the KV-type configuration and the SLS-type one set following WN optimization. Additionally, plot (e) and its inset from 22 to 25 s, plot (f), present the displacements for the primary system using KV-type TMD, SLS-type TMD with white noise (WN) optimization and SLS-type TMD with KT filter optimization.

tems (KV- and SLS-type) outperform the uncontrolled structure, with the SLS-type showing superior mitigation of the second DoF response, achieving up to nearly 30% reduction in peak displacement and 13% in peak acceleration, confirming the effectiveness of the proposed optimization strategy also in non-linear regimes.

## 5 | Conclusions

Mass damping systems have long been proven effective in mitigating the dynamic response of civil engineering structures. Traditional TMDs typically characterised by a low primary-to-secondary mass ratio (generally below 1%), offer limited performance under strong and impulsive seismic excitations. Recent advances have introduced non-conventional configurations with larger mass ratios, for example, IIS and MSCS. The practical implementation of such solutions is enabled by advances in isolation hardware, which allow for controlled dynamic coupling and decoupling of structural subsystems, reducing overall responses. These innovations, particularly when involving viscoelastic components, require more general modelling frameworks to accurately capture complex mechanical and time-dependent behaviours.



10969845, 2025, 12, Downloaded from https://onlinelibrary.wiley.com/doi/10.1002/eqe.70025 by Uni Federico II Di Napoli, Wiley Online Library on [17/10/2025]. See the Terms and Conditions (https://onlinelibrary.wiley.com/terms-and-conditions) on Wiley Online Library for rules of use; OA articles are governed by the applicable Creative Commons License

This study generalises classical viscously damped TMDs by replacing the KV model with the SLS one, introducing a new set of non-dimensional design parameters, namely two stiffness ratios and a relaxation parameter. This enhanced formulation allows for a more accurate and flexible representation of viscoelastic damping, addressing current limitations in TMD optimization under realistic seismic conditions.

The main key contributions and results are summarised here:

- Model generalisation:
  - classical KV-type TMDs are extended by incorporating the SLS model, introducing two stiffness ratios and a relaxation parameter;
  - the SLS-TMD asymptotically converges to the KV-TMD as the relaxation time approaches zero, thereby generalizing existing formulations.
- Optimization strategy:
  - the optimization problem is formulated as the minimization of the variance of the displacement of the primary system, by assuming the stiffness ratios and the relaxation dimensionless time as design parameters, given the mass ratio, the frequency and the damping of the primary structure;
  - damping of the primary system and coloured excitation spectra are explicitly and directly considered, being these factors typically overlooked in the existing literature;
  - closed-form solutions for optimal design parameters are derived under the hypothesis of white noise excitation and negligible primary damping, recovering the case analysed by Asami et al. [48], by instead adopting a different set of design parameters;
  - a numerical optimization enhancement is proposed for cases involving non-negligible damping in both primary and secondary masses.
- Performance under white noise excitation:
  - the optimally tuned SLS-TMD achieves up to 15% reduction in peak response compared to KV-TMDs when an excitation with constant PSD is considered (see Figures 8 and S1 of the Supporting Material).
- Validation via time-history analysis through lumped mass models subjected to seven natural seismic accelerograms:
  - ∼ 60% reduction in peak displacement compared to the uncontrolled system (see Figures 9 and S2 of the Supporting Material);
  - ∼ 15% reduction with respect to the conventional KV-type counterpart (see Figures 9 and S2 of the Supporting Material);
- Coloured excitation and earthquake-specific inputs have been incorporated in the optimization strategy and the following findings can be assumed in the linear framework:
  - real-life earthquake excitations are modelled using KT filter to remove the strict and quite unrealistic white noise assumption;
  - as a result, a ∼ 20% additional peak reduction for SLS-TMDs under coloured input versus the same TMD configuration subjected to the white noise excitation (see Figure 12);
  - globally, a further ∼ 25% reduction compared to the KV-TMDs under the same coloured input scenario is registered (see Figure 12);
  - importantly, by uploading non-linear constitutive law for the primary mass, accounting for stiffness degradation damage-induced, time history analyses show that optimised TMDs outperform with respect to NC configurations, by also achieving better reductions of the second DoF response for the SLS-type one compared to the KV-type system (see Section 2 of the Supporting Material).

These outcomes confirmed that the amplitude and frequency content of the seismic input play a crucial and far from negligible role in determining the optimal configuration of these systems, demonstrating the importance of carefully accounting for the site's geotechnical and seismogenic soil characteristics. The proposed SLS-type TMD optimization framework is shown to be highly general and adaptable across a wide parameter space and various input spectra, effectively capturing the role of primary structure damping and the effects of viscoelastic coupling. Ongoing research extends this approach toward multi-objective optimization, multiple TMDs tuned to different vibration modes and performance assessment under non-stationary and multi-hazard scenarios, with the goal of enabling practical implementation through scaled prototypes and detailed finite element models, by also accounting for possible case-specific non-linear phenomena that can occur.

### Author Contributions

**Mario Argenziano:** conceptualisation, methodology, software, validation, formal analysis, investigation, data curation, writing – original draft, review and editing, visualisation. **Alessandro Palmeri:** conceptualisation, methodology, investigation, validation, review and editing. **Angelo Rosario Carotenuto:** methodology, validation, review and editing. **Elena Mele:** conceptualisation, methodology, review and editing, supervised the project. **Massimiliano Fraldi:** conceptualisation, methodology, review and editing, supervised the project and funding.

### Acknowledgements

M.A. acknowledges the support from 'SiciliAn MicronanOTecH Research And Innovation CEnter "SAMOTHRACE"' (MUR, PNRR-M4C2, ECS_00000022), spoke 3—University of Palermo 'S2-COMMs—Micro and Nanotechnologies for Smart & Sustainable Communities'. M.F. acknowledges the support of the Italian Ministry of University and Research (MUR) through the grant FIT4MEDROB (PNC0000007). A.R.C. acknowledges the financial support under the National Recovery and Resilience Plan (NRRP), Mission 4, Component 2, Investment 1.1, Call for tender No. 1409 published on 14.9.2022 by the Italian Ministry of University and Research (MUR), funded by the European Union—NextGenerationEU—Project Title P2022M3KKC MECHAVERSE—CUP E53D23017310001—Grant Assignment Decree No. 1385 adopted on 1.9.2023 by the Italian Ministry of University and Research (MUR). Mario Argenziano acknowledges the fruitful discussions with Professor Yoshiki Ikeda (Disaster Prevention Research Institute, Kyoto University, Kyoto, Japan). This manuscript was also conducted under the auspices of the Italian Group of Theoretical Mechanics GNFM-INdAM of the National Institute of High Mathematics.

Open access publishing facilitated by Universita degli Studi di Napoli Federico II, as part of the Wiley - CRUI-CARE agreement.



10969845, 2025, 12, Downloaded from https://onlinelibrary.wiley.com/doi/10.1002/eqe.70025 by Uni Federico II Di Napoli, Wiley Online Library on [17/10/2025]. See the Terms and Conditions (https://onlinelibrary.wiley.com/terms-and-conditions) on Wiley Online Library for rules of use; OA articles are governed by the applicable Creative Commons License

## Conflicts of Interest

The authors declare no conflicts of interest. Furthermore, the views and conclusions expressed in this paper are solely those of the authors and do not necessarily represent the views or positions of the organizations which they are affiliated with.

## Data Availability Statement

The data that support the findings of this study are available from the corresponding author upon reasonable request.

## References


1. Y. Tsuneki, S. Torii, K. Murakami, and T. Sueoka, "Middle-Story Isolated Structural System of High-Rise Building," in *The 14th World Conference on Earthquake Engineering* (2008), https://doi.org/10.20965/jdr.2009.p0229.

2. S. J. Wang, K. C. Chang, J. S. Hwang, and B. H. Lee, "Simplified Analysis of Mid-Story Seismically Isolated Buildings," *Earthquake Engineering & Structural Dynamics* 40, no. 2 (2011): 119–133, https://doi.org/10.1002/eqe.1004.

3. G. Pipitone, G. Barone, and A. Palmeri, "Optimal Design of Double–Skin Façades as Vibration Absorbers," *Structural Control and Health Monitoring* 25 (2017): e2086, https://doi.org/10.1002/stc.2086.

4. G. Pipitone, G. Barone, and A. Palmeri, "Stochastic Design of Double-Skin Façades as Seismic Vibration Absorbers," *Advances in Engineering Software* 142 (2020): 102749, https://doi.org/10.1016/j.advengsoft.2019.102749.

5. M. Martinez-Paneda and A. Y. Elghazouli, "An Integrated Damping System for Tall Buildings," *Structural Design of Tall and Special Buildings* 29, no. 7 (2020): e1724, https://doi.org/10.1002/tal.1724.

6. C. Masnata, A. Di Matteo, C. Adam, and A. Pirrotta, "Assessment of the Tuned Mass Damper Inerter for Seismic Response Control of Base-Isolated Structures," *Structural Control and Health Monitoring* 28, no. 2 (2021): e2665, https://doi.org/10.1002/stc.2665.

7. E. Mele, D. Faiella, and M. Argenziano, "Innovative Mass-Damping-Based Approaches for Seismic Design of Tall Buildings," in *Proceedings of the 8th International Conference on Computational Methods in Structural Dynamics and Earthquake Engineering* (COMPDYN 2021) (Eccomas Proceedia, Paper ID 8598, pp. 1778–1792), https://doi.org/10.7712/120121.8598.18959.

8. Y. Ikeda, "Fundamental Equation Based on Pole Allocation for Inter-story Seismic Isolation of Buildings," *Structural Control and Health Monitoring* 28, no. 3 (2021): e2687, https://doi.org/10.1002/stc.2687.

9. D. Faiella, M. Argenziano, and E. Mele, "Improving the Seismic Response of Tall Buildings: From Diagrid to Megastructures and Mega-Subcontrol Systems," *Open Construction & Building Technology Journal* 16, no. 1 (2022), https://doi.org/10.2174/18748368-v16-e2201030.

10. F. Esposito, M. Argenziano, D. Faiella, and E. Mele, "Intermediate Isolation System With Nonlinear Lower Structure and Isolation System," *Applied Sciences* 13, no. 7 (2023): 4590, https://doi.org/10.3390/app13074590.

11. J. P. Den Hartog, *Mechanical Vibrations* (Courier Corporation, 1985).

12. S. Randall, D. Halsted III, and D. Taylor, "Optimum Vibration Absorbers for Linear Damped Systems," *Journal of Mechanical Design* 103, no. 4 (1981): 908–913, https://doi.org/10.1115/1.3255005.

13. G. Warburton, "Optimum Absorber Parameters for Various Combinations of Response and Excitation Parameters," *Earthquake Engineering & Structural Dynamics* 10, no. 3 (1982): 381–401, https://doi.org/10.1002/eqe.4290100304.

14. H. C. Tsai and G. C. Lin, "Optimum Tuned-Mass Dampers for Minimizing Steady-State Response of Support-Excited and Damped Systems," *Earthquake Engineering & Structural Dynamics* 22, no. 11 (1993): 957–973, https://doi.org/10.1002/eqe.4290221104.

15. F. Sadek, B. Mohraz, A. W. Taylor, and R. M. Chung, "A Method of Estimating the Parameters of Tuned Mass Dampers for Seismic Applications," *Earthquake Engineering & Structural Dynamics* 26, no. 6 (1997): 617–635, https://doi.org/10.1002/(SICI)1096-9845(199706)26:6(617::AID-EQE664)3.0.CO;2-Z.

16. T. Asami, O. Nishihara, and A. M. Baz, "Analytical Solutions to H Infinity and H 2 Optimization of Dynamic Vibration Absorbers Attached to Damped Linear Systems," *Journal of Vibration and Acoustics* 124, no. 2 (2002): 284–295, https://doi.org/10.1115/1.1456458.

17. S. Krenk, "Frequency Analysis of the Tuned Mass Damper," *Journal of Applied Mechanics* 72, no. 6 (2005): 936–942, https://doi.org/10.1115/1.2062867.

18. S. Krenk and J. Høgsberg, "Tuned Mass Absorbers on Damped Structures Under Random Load," *Probabilistic Engineering Mechanics* 23, no. 4 (2008): 408–415, https://doi.org/10.1016/j.probengmech.2007.04.004.

19. A. Reggio and M. D. Angelis, "Optimal Energy-Based Seismic Design of Non-Conventional Tuned Mass Damper (TMD) Implemented via Inter-Story Isolation," *Earthquake Engineering & Structural Dynamics* 44, no. 10 (2015): 1623–1642, https://doi.org/10.1002/eqe.2548.

20. M. Argenziano, A. Cutolo, E. Babilio, A. Carotenuto, and M. Fraldi, "Moving Mass Over a Viscoelastic System: Asymptotic Behaviours and Insights Into Nonlinear Dynamics," *Nonlinear Dynamics* 111 (2023): 1–20, https://doi.org/10.1007/s11071-023-08465-z.

21. S. Chowdhury, A. Banerjee, and S. Adhikari, "Enhancing Seismic Resilience of Nonlinear Structures Through Optimally Designed Additional Mass Dampers," *International Journal of Non-Linear Mechanics* 162 (2024): 104717, https://doi.org/10.1016/j.ijnonlinmec.2024.104717.

22. K. Kwok and B. Samali, "Performance of Tuned Mass Dampers Under Wind Loads," *Engineering Structures* 17, no. 9 (1995): 655–667, https://doi.org/10.1016/0141-0296(95)00035-6.

23. L. Zuo and S. A. Nayfeh, "Optimization of the Individual Stiffness and Damping Parameters in Multiple-Tuned-Mass-Damper Systems," *Journal of Vibration and Acoustics* 127, no. 1 (2005): 77–83, https://doi.org/10.1115/1.1855929.

24. M. Fraldi, A. Cugno, L. Deseri, K. Dayal, and N. Pugno, "A Frequency-Based Hypothesis for Mechanically Targeting and Selectively Attacking Cancer Cells," *Journal of the Royal Society Interface* 12, no. 111 (2015): 20150656, 10.1098/rsif.2015.0656.

25. M. Fraldi, A. Cutolo, A. R. Carotenuto, S. Palumbo, and N. Pugno, "A Lesson From Earthquake Engineering for Selectively Damaging Cancer Cell Structures," *Journal of the Mechanical Behavior of Biomedical Materials* 119 (2021): 104533, 10.1016/j.jmbbm.2021.104533.

26. F. Pellizzari, G. Marano, A. Palmeri, R. Greco, and M. Domaneschi, "Robust Optimization of MTMD Systems for the Control of Vibrations," *Probabilistic Engineering Mechanics* 70 (2022): 103347, https://doi.org/10.1016/j.probengmech.2022.103347.

27. A. Cutolo, A. R. Carotenuto, M. A. Cutolo, et al., "Ultrasound Waves in Tumors via Needle Irradiation for Precise Medicine," *Scientific Reports* 12, no. 1 (2022): 6513, https://doi.org/10.1038/s41598-022-10407-5.

28. G. Magliulo and D. D'Angela, "Seismic Response and Capacity of Inelastic Acceleration-Sensitive Nonstructural Elements Subjected to Building Floor Motions," *Earthquake Engineering & Structural Dynamics* 53, no. 4 (2024): 1421–1445, https://doi.org/10.1002/eqe.4080.

29. M. Argenziano, E. Babilio, Y. Ikeda, and M. Fraldi, "A *Heretical* Point of View in Masonry Structures Dynamics," *Royal Society Open Science* 12, no. 4 (2025): 241148, https://doi.org/10.1098/rsos.241148.

30. M. Argenziano, M. Zingales, A. Cutolo, E. Bologna, and M. Fraldi, "Competition Between Elasticity and Adhesion in Caterpillar Locomotion," *Journal of the Royal Society Interface* 22, no. 225 (2025): 20240703, https://doi.org/10.1098/rsif.2024.0703.

31. A. A. Markou and G. D. Manolis, "A Fractional Derivative Zener Model for the Numerical Simulation of Base Isolated Structures," *Bulletin*




10969845, 2025, 12, Downloaded from https://onlinelibrary.wiley.com/doi/10.1002/eqe.70025 by Uni Federico II Di Napoli, Wiley Online Library on [17/10/2025]. See the Terms and Conditions (https://onlinelibrary.wiley.com/terms-and-conditions) on Wiley Online Library for rules of use; OA articles are governed by the applicable Creative Commons License

*of Earthquake Engineering* 14 (2016): 283–295, https://doi.org/10.1007/s10518-015-9801-7.

32. C. G. Koh and J. M. Kelly, "Application of Fractional Derivatives to Seismic Analysis of Base-Isolated Models," *Earthquake Engineering & Structural Dynamics* 19, no. 2 (1990): 229–241, https://doi.org/10.1002/eqe.4290190207.

33. F. Naeim and J. M. Kelly, *Design of Seismic Isolated Structures: From Theory to Practice* (John Wiley & Sons, 1999).

34. T. T. Soong and G. F. Dargush, *Passive Energy Dissipation Systems in Structural Engineering* (Wiley, 1997).

35. G. Barone, M. Di Paola, F. L. Iacono, and G. Navarra, "Viscoelastic Bearings With Fractional Constitutive Law for Fractional Tuned Mass Dampers," *Journal of Sound and Vibration* 344 (2015): 18–27, https://doi.org/10.1016/j.jsv.2015.01.017.

36. A. Rashid and C. M. Nicolescu, "Design and Implementation of Tuned Viscoelastic Dampers for Vibration Control in Milling," *International Journal of Machine Tools and Manufacture* 48, no. 9 (2008): 1036–1053, https://doi.org/10.1016/j.ijmachtools.2007.12.013.

37. J. Dai, Z. D. Xu, and P. P. Gai, "Dynamic Analysis of Viscoelastic Tuned Mass Damper System Under Harmonic Excitation," *Journal of Vibration and Control* 25, no. 11 (2019): 1768–1779, https://doi.org/10.1177/1077546319833888.

38. J. Dai, Z. D. Xu, P. P. Gai, and Z. W. Hu, "Optimal Design of Tuned Mass Damper Inerter With a Maxwell Element for Mitigating the Vortex-Induced Vibration in Bridges," *Mechanical Systems and Signal Processing* 148 (2021): 107180, https://doi.org/10.1016/j.ymssp.2020.107180.

39. A. Palmeri, F. Ricciardelli, A. De Luca, and G. Muscolino, "State Space Formulation for Linear Viscoelastic Dynamic Systems With Memory," *Journal of Engineering Mechanics* 129, no. 7 (2003): 715–724, https://doi.org/10.1061/(ASCE)0733-9399(2003)129:7(7.

40. A. Palmeri, F. Ricciardelli, G. Muscolino, and A. De Luca, "Effects of Viscoelastic Memory on the Buffeting Response of Tall Buildings," *Wind and Structures* 7, no. 2 (2004): 89–106, https://doi.org/10.12989/was.2004.7.2.089.

41. A. Palmeri, F. Ricciardelli, G. Muscolino, and A. De Luca, "Random Vibration of Systems With Viscoelastic Memory," *Journal of Engineering Mechanics* 130, no. 9 (2004): 1052–1061, https://doi.org/10.1061/(ASCE)0733-9399(2004)130:9(1052.

42. J. Woodhouse, "Linear Damping Models for Structural Vibration," *Journal of Sound and Vibration* 215, no. 3 (1998): 547–569, https://doi.org/10.1006/jsvi.1998.1709.

43. S. Adhikari and J. Woodhouse, "Identification of Damping: Part 1, Viscous Damping," *Journal of Sound and vibration* 243, no. 1 (2001): 43–61, https://doi.org/10.1006/jsvi.2000.3391.

44. S. Adhikari and J. Woodhouse, "Identification of Damping: Part 2, Non-Viscous Damping," *Journal of Sound and Vibration* 243, no. 1 (2001): 63–88, https://doi.org/10.1006/jsvi.2000.3392.

45. N. Makris and J. Zhang, "Time-Domain Viscoelastic Analysis of Earth Structures," *Earthquake Engineering & Structural Dynamics* 29, no. 6 (2000): 745–768, https://doi.org/10.1002/(SICI)1096-9845(200006)29:6⟨745::AID-EQE937⟩3.0.CO;2-E.

46. S. Chowdhury, A. Banerjee, and S. Adhikari, "The Optimum Enhanced Viscoelastic Tuned Mass Dampers: Exact Closed-Form Expressions," *Journal of Vibration and Control* 30, no. 5-6 (2024): 1080–1102, https://doi.org/10.1177/10775463231156240.

47. T. Asami and O. Nishihara, "Analytical and Experimental Evaluation of an Air Damped Dynamic Vibration Absorber: Design Optimizations of the Three-Element Type Model," *Journal of Vibration and Acoustics* 121, no. 3 (1999): 334–342, https://doi.org/10.1115/1.2893985.

48. T. Asami and O. Nishihara, "H 2 Optimization of the Three-Element Type Dynamic Vibration Absorbers," *Journal of Vibration and Acoustics* 124, no. 4 (2002): 583–592, https://doi.org/10.1115/1.1501286.

49. Z. D. Xu, "Earthquake Mitigation Study on Viscoelastic Dampers for Reinforced Concrete Structures," *Journal of Vibration and Control* 13, no. 1 (2007): 29–43, https://doi.org/10.1177/1077546306068058.

50. Z. D. Xu, C. Xu, and J. Hu, "Equivalent Fractional Kelvin Model and Experimental Study on Viscoelastic Damper," *Journal of Vibration and Control* 21, no. 13 (2015): 2536–2552, https://doi.org/10.1177/1077546313513360.

51. C. I. Muresan, E. H. Dulf, and O. Prodan, "A Fractional Order Controller for Seismic Mitigation of Structures Equipped With Viscoelastic Mass Dampers," *Journal of Vibration and Control* 22, no. 8 (2016): 1980–1992, https://doi.org/10.1177/1077546314557553.

52. A. Batou and S. Adhikari, "Optimal Parameters of Viscoelastic Tuned-Mass Dampers," *Journal of Sound and Vibration* 445 (2019): 17–28, https://doi.org/10.1016/j.jsv.2019.01.010.

53. J. Dai, Z. D. Xu, P. P. Gai, and H. W. Li, "Effect of Frequency Dependence of Large Mass Ratio Viscoelastic Tuned Mass Damper on Seismic Performance of Structures," *Soil Dynamics and Earthquake Engineering* 130 (2020): 105998, https://doi.org/10.1016/j.soildyn.2019.105998.

54. M. Argenziano, E. Mele, and A. Palmeri, "Optimal Design of Viscoelastic Tuned Mass Dampers for Structures Exposed to Coloured Excitations," in A. Zingoni (Ed.), Current Perspectives and New Directions in Mechanics, Modelling and Design of Structural Systems (Proceedings of the Eighth International Conference on Structural Engineering, Mechanics and Computation, SEMC 2022). (CRC Press, 2022), 63–69, https://doi.org/10.1201/9781003348450-10.

55. R. Christensen, *Theory of Viscoelasticity: An Introduction* (Elsevier, 2012).

56. A. Palmeri and G. Muscolino, "Response of Beams Resting on Viscoelastically Damped Foundation to Moving Oscillators," *International Journal of Solids and Structures* 44, no. 5 (2007): 1317–1336, https://doi.org/10.1016/j.ijsolstr.2006.06.013.

57. G. Muscolino, *Dinamica delle strutture* (McGraw-Hill, 2002).

58. L. Meirovitch, *Fundamentals of Vibrations* (Waveland Press, 2010).

59. M. Argenziano, D. Faiella, A. Carotenuto, E. Mele, and M. Fraldi, "Generalization of the Den Hartog Model and Rule-of-Thumb Formulas for Optimal Tuned Mass Dampers," *Journal of Sound and Vibration* 538 (2022): 117213, https://doi.org/10.1016/j.jsv.2022.117213.

60. S. H. Crandall and W. D. Mark, *Random Vibration in Mechanical Systems* (Academic Press, 2014).

61. C. F. Van Loan, "The Ubiquitous Kronecker Product," *Journal of Computational and Applied Mathematics* 123, no. 1 (2000): 85–100, https://doi.org/10.1016/S0377-0427(00)00393-9.

62. MATLAB, version 9.8 (R2020a) (MathWorks Inc., 2020).

63. D. E. Goldberg, *Genetic Algorithms in Search, Optimization, and Machine Learning* (Addison-Wesley, 1989).

64. A. R. Conn, N. I. Gould, and P. Toint, "A Globally Convergent Augmented Lagrangian Algorithm for Optimization With General Constraints and Simple Bounds," *SIAM Journal on Numerical Analysis* 28, no. 2 (1991): 545–572, https://doi.org/10.1137/0728030.

65. A. Conn, N. Gould, and P. Toint, "A Globally Convergent Lagrangian Barrier Algorithm for Optimization With General Inequality Constraints and Simple Bounds," *Mathematics of Computation* 66, no. 217 (1997): 261–288, https://doi.org/10.1090/S0025-5718-97-00777-1.

66. J. Kennedy and R. Eberhart, "Particle Swarm Optimization," in *Proceedings of ICNN'95-International Conference on Neural Networks* (1995), 1942–1948, https://doi.org/10.1109/ICNN.1995.488968.

67. E. Mezura-Montes and C. A. C. Coello, "Constraint-Handling in Nature-Inspired Numerical Optimization: Past, Present and Future," *Swarm and Evolutionary Computation* 1, no. 4 (2011): 173–194, https://doi.org/10.1016/j.swevo.2011.10.001.



10969945, 2025, 12, Downloaded from https://onlinelibrary.wiley.com/doi/10.1002/eqe.70025 by Uni Federico II Di Napoli, Wiley Online Library on [17/10/2025]. See the Terms and Conditions (https://onlinelibrary.wiley.com/terms-and-conditions) on Wiley Online Library for rules of use; OA articles are governed by the applicable Creative Commons License

68. M. E. H. Pedersen, *Good Parameters for Particle Swarm Optimization*, Technical Report HL1001 (Hvass Lab., 2010), 1551–3203, https://doi.org/10.13140/RG.2.2.23771.49445.

69. Computers and Structures Inc. (CSI), *SAP2000: Integrated Software for Structural Analysis and Design* (Computers and Structures Inc., 2013).

70. K. Kanai, "Semi-Empirical Formula for the Seismic Characteristics of the Ground," *Bulletin of the Earthquake Research Institute* 35 (1957): 309–325.

71. H. Tajimi, "A Statistical Method of Determining the Maximum Response of a Building Structure During an Earthquake," in *2nd World Conference on Earthquake Engineering* (1960), 781–797.

72. S. J. Hormozabad and M. G. Soto, "Seismic Design Optimization of Controlled Rocking Steel Braced Frames Based on Neural Dynamic Model," in *17th World Conference on Earthquake Engineering* (2020).

73. S. S. P. Lai, "Statistical Characterization of Strong Ground Motions Using Power Spectral Density Function," *Bulletin of the Seismological Society of America* 72, no. 1 (1982): 259–274, https://doi.org/10.1785/BSSA0720010259.

## Supporting Information

Additional supporting information can be found online in the Supporting Information section.

Supporting Information



10969845, 2025, 12, Downloaded from https://onlinelibrary.wiley.com/doi/10.1002/eqe.70025 by Uni Federico II Di Napoli, Wiley Online Library on [17/10/2025]. See the Terms and Conditions (https://onlinelibrary.wiley.com/terms-and-conditions) on Wiley Online Library for rules of use; OA articles are governed by the applicable Creative Commons License